CB NOTE 318

Pseudoscalars decaying into $\eta\pi\pi$.

David Bugg, Nana Djaoshvili, Jan Kisiel
Lucien Montanet, Rafik Ouared

9 November 1997
CERN

Contents

1 Introduction.

The first evidence for a pseudoscalar state with a mass around 1400 MeV/c^2 comes from the CERN-Collège de France experiment [1] who studied $\bar{p}p$ annihilation at rest into $K\bar{K}\pi\pi\pi$ and observed an enhancement in the $(K\bar{K}\pi)$ neutral system with a mass of 1425 ± 7 MeV/c^2 and a width of 80 ± 10 MeV/c^2,called E meson. Later, a resonance named ι, with the same quantum numbers, mass and width, was observed in J/ψ radiative decay [2]. This made the E/ι a prime pseudoscalar glueball candidate. However the quarkonium interpretation still has supporters, the E/ι being often taken as one of the first radial excitation of η or η'. Most of the previous measurements were made on the $K\bar{K}\pi$ decay mode of the E/ι. The noticeable exception is the work of D.Urner [3], [4]. He observed the $\eta\pi\pi$ decay mode of E in the analysis of high statistics data on $\bar{p}p \to \pi^+\pi^-\eta 2\pi^0$ taken with a dedicated trigger.

As we are dealing with $\bar{p}p$ annihilations at rest in LH_2 (dominated by $^1S_0$ and $^3S_1$ initial states of protonium), the simplest experimental way to look for pseudoscalars is to study the following transition

$$0^{-+} \;\to\; 0^{-+} + 0^{++}, \tag{1}$$

where 0^{++} will be materialized by a pair of pions ($\pi^0\pi^0$ or $\pi^+\pi^-$) in S-wave. Therefore, to study the $\eta\pi\pi$ decay mode of 0^{-+} (I=0) states, one has to investigate the following 5-body annihilations:

$$\bar{p}p \;\to\; \eta 4\pi, \tag{2}$$

with three possibilities for the 4π system:

$$\bar{p}p \;\to\; \eta 4\pi^0, \tag{3}$$

$$\bar{p}p \;\to\; \eta\pi^+\pi^- 2\pi^0, \tag{4}$$

$$\bar{p}p \;\to\; \eta 2\pi^+ 2\pi^-. \tag{5}$$

Reaction (3) is being analyzed by the Bonn group. Reaction (4) has been studied by D.Urner (see above). In this note we will discuss reaction (5). The CB data allows to study reactions (3) and (4) with large statistics. This is not the case for reaction (5). However reaction (3) suffers from a large combinatorial background (10γ final state) and reaction (4) from a large $\omega\eta\pi$ background. Reaction (5) is of course not free from background, but, as we will see, its elimination turned out to be easy.

Criterium	number of events [M]
4-prongs triggered	9.38
4-gold tracks (Σq_i=0)	2.54
4-gold tracks, $n\gamma^*$, n=0-24	1.28

Table 1: *Summary of data selection.*

To study reaction (5) we consider the following decay modes of the $\eta(547)$:

$$\bar{p}p \rightarrow \eta 2\pi^+2\pi^-, \eta \rightarrow 2\gamma, \tag{6}$$

$$\bar{p}p \rightarrow \eta 2\pi^+2\pi^-, \eta \rightarrow 3\pi^0 \rightarrow 6\gamma, \tag{7}$$

$$\bar{p}p \rightarrow \eta\pi^+\pi^-2\pi^0, \eta \rightarrow \pi^+\pi^-\pi^0. \tag{8}$$

2 Analysis of reaction $\bar{p}p \rightarrow \eta 2\pi^+2\pi^-, \eta \rightarrow 2\gamma$.

2.1 Data selection.

The analysis of reaction (6) is based on $\sim$ 9.4M triggered 4-prong events: 2.1M from Jun91, 1.0M from Aug91 and 6.28M from Apr96. We select $\sim$ 2.5M events with 4 'golden' tracks (according to the usual definition) which conserve charge. For the gamma's (which will be called γ^*'s) we request unmatched peds with at least 10MeV energy. Events with peds for which the central crystal is of type-13 are rejected. This reduces the sample of 2.5M events to $\sim$ 1.3M.

The table 1 gives the number of events at every selection step. 1.26M events with 4 'golden' tracks and 2 or more γ^* were submitted to the 4C fit (energy and momentum conservation) hypothesis $2\pi^+2\pi^-2\gamma$. 208K events survived a 10% CL cut and for them, the $\gamma\gamma$ invariant mass distribution is plotted in fig. 1 One can see two well separated peaks corresponding to the π^0 and η mesons, and a low energy residual background due to split-offs. The η peak has a mass of 548.3MeV/c^2, in good agreement with PDG value. It is background free. We observe 4006 $2\pi^+2\pi^-\eta$ events. The corresponding number of $2\pi^+2\pi^-\pi^0$ events is equal to 178032.

The 5C kinematic fit hypothesis to the reaction $\bar{p}p \rightarrow 2\pi^+2\pi^-\eta$ ($\eta \rightarrow 2\gamma$) and $\bar{p}p \rightarrow 2\pi^+2\pi^-\pi^0$ ($\pi^0 \rightarrow 2\gamma$) has been performed on these 208K events. 4020 $2\pi^+2\pi^-\eta$ events and 176484 $2\pi^+2\pi^-\pi^0$ passed through CL$>$ 0.1. Fig. 2 shows the CL distribution for the $2\pi^+2\pi^-\eta$ hypothesis whereas fig. 3 shows the pulls of the kinematic fit. A Maximum Detectable Momentum (MDM)[8] of $-$20GeV/c has been applied to correct for charged momenta. The number of $2\pi^+2\pi^-\eta$ and $2\pi^+2\pi^-\pi^0$ events from the 5C fit is in good agreement with the direct observation made in fig. 1.

2.2 Branching ratio for the reaction $\bar{p}p \to \eta 2\pi^+ 2\pi^-$.

100K Monte Carlo events (phase space) have been generated for reactions (5) and for

$$\bar{p}p \quad \to \quad \pi^0 2\pi^+ 2\pi^-, \pi^0 \to 2\gamma. \tag{9}$$

With the selection criteria discussed above, including a 10% CL cut on 5C fits, we obtain a reconstruction efficiency of 6.8% and 6.4% for reactions (6) and (9), respectively. Using the known branching ratio BR($\bar{p}p \to \pi^0 2\pi^+ 2\pi^-$) = $17.3 \pm 1.5\%$ [5] we find the BR for reaction (5)

$$BR(\bar{p}p \to \eta 2\pi^+ 2\pi^-) \quad = \quad 17.3\% \times \frac{4020}{176484} \times \frac{98.8\%}{39.25\%} \times \frac{6.4\%}{6.8\%} = (0.9 \pm 0.15)\%. \tag{10}$$

2.3 Qualitative description of reaction $\bar{p}p \to \eta 2\pi^+ 2\pi^-, \eta \to 2\gamma$.

Fig. 4 shows the $\eta\pi^\pm$ effective mass distribution (4 combinations per event). One may see a week production of $a_0(980)$. Fig. 5 shows the $\eta\pi^+\pi^-$ effective mass distribution (for 4 combinations per events); on the same figure the $\eta\pi^-\pi^-/\eta\pi^+\pi^+$ mass distribution is also shown. We note the presence of the $\eta'(958)$ and a shoulder at 1400 MeV/c^2, as already observed by D.Urner who was studying reaction (4). The other invariant mass distributions like 3π or 4π do not show additional significant signals.

2.4 The asymmetry parameter R.

The phase space for the $\eta\pi^+\pi^-$ distribution peaks at $\sim$ 1200MeV. If a narrow $\eta\pi^+\pi^-$ resonance has a mass, much smaller or much larger than 1200 MeV, it will introduce an asymmetry in the kinematics of the $\pi^+\pi^-$ pairs which come either from the decay of the resonance or from the pion system recoiling against this resonance. To make use of this effect, we introduce an asymmetry parameter R defined in the following way:

$$R \quad = \quad \frac{P_{\pi^+{}_i} + P_{\pi^-{}_i}}{P_{\pi^+{}_j} + P_{\pi^-{}_j}}, \quad i,j = 1,2 \tag{11}$$

where P is equal to $\sqrt{P_x^2 + P_y^2 + P_z^2}$. Out of the four possible combinations in $\eta\pi^+\pi^-$ spectrum, only one may come from a narrow resonance. Let's call the pions from the decay of this resonance π_R and $\pi_{\bar{R}}$ those which do not come from the decay of the resonance. We can now define four $\eta\pi^+\pi^-$ combinations: the 'resonant combination' $\eta\pi^+{}_R\pi^-{}_R$, the 'direct reflection' $\eta\pi^+{}_{\bar{R}}\pi^-{}_{\bar{R}}$ and two 'crossing combinations' $\eta\pi^+{}_R\pi^-{}_{\bar{R}}$, $\eta\pi^+{}_{\bar{R}}\pi^-{}_R$. The four corresponding asymmetry parameters are:

reaction	n_{ev} observed	ϵ[%]	BR($\bar{p}p$)[%]
$\bar{p}p \to \eta\pi^+\pi^-\pi^+\pi^-$	4020	6.54	0.90 ± 0.15
	$\eta \to \gamma\gamma$		
$\bar{p}p \to \eta'\pi^+\pi^-$	700 ± 40	5.5	0.42 ± 0.03
	$\eta' \to \eta\pi^+\pi^-$		
	$\eta \to \gamma\gamma$		
$\bar{p}p \to E\sigma$	700 ± 100	6.8	0.32 ± 0.05
	$E \to \eta\sigma$		
	$\eta \to \gamma\gamma$		
	$\sigma \to \pi^+\pi^-$		
$\bar{p}p \to \eta\sigma\sigma$	2600 ± 150	6.8	1.26 ± 0.13

Table 2: *Summary of results.* n_{ev} *is the number of observed events, and* ϵ *the overall efficiency. The Branching Ratios of* $\eta \to \gamma\gamma$, $\eta' \to \eta\pi^+\pi^-$ *and* $\sigma \to \pi^+\pi^-$ *have been taken into account.*

$$R_1 = \frac{P_{\pi^+{}_R} + P_{\pi^-{}_R}}{P_{\pi^+{}_{\bar{R}}} + P_{\pi^-{}_{\bar{R}}}}; \qquad \frac{1}{R_1};$$
$$R_2 = \frac{P_{\pi^+{}_R} + P_{\pi^-{}_{\bar{R}}}}{P_{\pi^+{}_{\bar{R}}} + P_{\pi^-{}_R}}; \qquad \frac{1}{R_2}. \tag{12}$$

We call symmetric events, events with values of R_1 and R_2 between α and $1/\alpha$, where α is a parameter. The asymmetric events have at least one value of $R_i, (i = 1, 2)$ outside this interval. To split the sample of events into two groups (symmetric and asymmetric) we varied the parameter α in steps of 0.05 and defined the best value of α as the value which 'leaves' all $\eta'(958)$ events in one group. We used the η' resonance as the best known narrow state to calibrate the method. We found that for asymmetric events only one of the two ratios R_1 and R_2 is outside the (α-$1/\alpha$) interval.

Fig. 6 shows the $\eta\pi^+\pi^-$ invariant mass for asymmetric events (histogram) and for symmetric ones (crosses) for the value of $\alpha = 0.6$. Fig. 7 shows the invariant mass distribution for the asymmetric events but only for the non-crossing combinations (2 combinations per event). The crosses show the expected behaviour of this distribution for the phase space events with the same cut on α. The data and MC samples have been normalized to the same number of entries before cutting on α. One can see η' and E meson signals together with their direct reflections. To eliminate the reflection of the η', we reject the events with the invariant mass $m(\eta\pi^+\pi^-) = 958 \pm 15$ MeV/c^2. Fig. 8 shows the $\eta\pi^+\pi^-$ spectrum without the η' reflection in the E/ι region.

Using the same value of α (α=0.6), we obtain an enhancement at 1295 MeV/c^2 in the $\eta\pi^+\pi^-$ invariant mass spectrum for the symmetric events, as shown in figure 9. The crosses show the expected distribution for the phase space with the same cut on α.

Fig. 10 shows the scatter plot $m(\pi^+\pi^-)$ versus $m(\pi^+\pi^-)$ (2 combinations per event) for symmetric events. We see accumulations which can be interpreted in two ways at

least, either as a relatively narrow object ($\Gamma < 100$ MeV) around 500 MeV/c^2 or as a broad ($\Gamma \sim 300$ MeV) concentration of $\pi^+\pi^-$ events centered at 600 MeV/c^2. Assuming a negligible ρ effect, these accumulations could be interpreted in terms of a relatively narrow $\eta\pi\pi$ resonance. Fig. 11 shows the same scatter plot for phase space. The difference with fig. 10 is obvious.

Fig. 12 shows the $\eta\pi^+\pi^-$ mass distribution after combining the η from each event with the $\pi^+\pi^-$ combination corresponding to the broad structure and the $\eta\pi^+\pi^-$ mass distribution which combines the same η with the narrow $\pi^+\pi^-$ structure. The first histogram is a Breit-Wigner distribution with 600 ± 100 events, centered at 1295 MeV/c^2 with a 65 MeV/c^2 width, whereas the second histogram can be regarded as the direct reflection of this Breit-Wigner. We conclude from these observations that the upper limit for the production of $\eta(1295)$ is $(0.26 \pm 0.06)\%$ taking into account the σ decay into $\pi^+\pi^-$. Table 2 gives a quantitative estimation of the various final states which contribute to reaction (6). These contributions have been added incoherently. The Monte Carlo simulation shows that reconstruction efficiences are similar for all channels and equal to $\sim$6.7%, except for $\eta'\pi^+\pi^-$ channel ($\sim$5.5%). The mass, width and BR($\bar{p}p \to E\pi^+\pi^-, E \to \eta\pi^+\pi^-$) are in excellent agreement with values obtained by D.Urner [4].

3 Analysis of reaction $\bar{p}p \to 2\pi^+2\pi^-\eta, \eta \to 3\pi^0 \to 6\gamma$.

Data selection for reaction (7) follows the procedure applied to reaction (6). A 4C fit to the hypothesis $2\pi^+2\pi^-6\gamma$ was performed on 848K events with 4 golden tracks and 6 or more γ*. 7946 events survived through a 10% CL cut. These events have then been submitted to 7C fit for the hypothesis $\bar{p}p \to 2\pi^+2\pi^-3\pi^0, \pi^0 \to 2\gamma$ and 6040 events survived through a 10% CL cut. Fig. 13 shows the PED and γ* multipliciplicities for these 6040 events whereas fig. 14 shows the pulls for this reaction. Up to 15 combinations of six γ's may give a fit to the hypothesis $2\pi^+2\pi^-3\pi^0$, but we observed that only one of them has a probability greater than 10%. Fig. 15 shows the $3\pi^0$ invariant mass for 6040 events with CL>10%. The η signal comes up very clearly, however contrairily to the $2\pi^+2\pi^-\eta, \eta \to 2\gamma$ channel, the $\eta \to 3\pi^0$ sits now on a background. Indeed there are other channels which contribute to the $2\pi^+2\pi^-3\pi^0$ final state, namely $\omega\omega\pi^0$ ($\omega \to \pi^+\pi^-\pi^0$), $\omega\eta\pi^0$ ($\omega, \eta \to \pi^+\pi^-\pi^0$), and to a lesser extend $\eta\eta\pi^0$ ($\eta \to \pi^+\pi^-\pi^0$) and $\pi^+\pi^-2\pi^0\eta$ ($\eta \to \pi^+\pi^-\pi^0$). We perform kinematic fits for these background channels and select only these events which give a fit probability less then 10% to each background channel and greater than 10% to $2\pi^+2\pi^-\eta, \eta \to 3\pi^0$ hypothesis. Tab. 3 gives the selection and reconstruction efficiency for reaction (7), as well as for reaction $\bar{p}p \to \eta'\pi^+\pi^-, \eta' \to \pi^+\pi^-\eta, \eta \to 3\pi^0$, and the corresponding numbers of events (after 10% CL cut).

The branching ratio for reaction $\bar{p}p \to \eta\pi^+\pi^-\pi^+\pi^-, \eta \to 3\pi^0$ (see tab.3) can be compared with the branching ratio for the same reaction but with $\eta \to \gamma\gamma$ (see tab.2). There is a good agreement between these two measurements.

reaction	n_{ev} observed	ϵ[%]	BR($\bar{p}p$)[%]
$\bar{p}p \to \eta\pi^+\pi^-\pi^+\pi^-$	1200 ± 100	2.3	0.97 ± 0.1
	$\eta \to 3\pi^0$		
$\bar{p}p \to \eta'\pi^+\pi^-$	140 ± 30	1.5	0.39 ± 0.08
	$\eta' \to \eta\pi^+\pi^-$		
	$\eta \to 3\pi^0$		

Table 3: *Summary of results from reaction (7). For details the caption of tab.2.*

reaction	n_{ev} observed	ϵ[%]	BR($\bar{p}p$)[%]
$\bar{p}p \to \eta\pi^+\pi^-\pi^0\pi^0$	373 ± 50	1.3	0.8 ± 0.3
	$\eta \to \pi^+\pi^-\pi 0$		
$\bar{p}p \to \eta'\pi^+\pm$	40 ± 5	1.3	0.37 ± 0.05
	$\eta' \to \eta\pi^0\pi^0$		
	$\eta \to \pi^+\pi^-\pi^0$		
$\bar{p}p \to \eta'\pi^0\pi^0$	22 ± 3	1.3	0.11 ± 0.03
	$\eta' \to \eta\pi^+\pi^-$		
$\eta \to \pi^+\pi^-\pi^0$			

Table 4: *Summary of results from reaction $\bar{p}p \to \pi^+\pi^-2\pi^0\eta, \eta \to \pi^+\pi^-\pi^0$. For details see caption of the fig.2.*

4 Analysis of reaction $\bar{p}p \to \pi^+\pi^-2\pi^0\eta, \eta \to \pi^+\pi^-\pi^0$.

The same final state $2\pi^+2\pi^-3\pi^0$ as studied in sec.3 can provide information on reaction (8) where $\eta \to \pi^+\pi^-\pi^0$. The selection criteria for this reaction are exactly the same as for reaction (7). The evidence for $\eta \to \pi^+\pi^-\pi^0$ in reaction (8) is shown in fig. 16, where $\pi^+\pi^-\pi^0$ invariant mass is plotted (12 combinations per event). We observe 784 $\eta \to \pi^+\pi^-\pi^0$ out of which 411 come from the following two reactions:

$$\bar{p}p \quad \to \quad \omega\eta\pi^0, \omega, \eta \to \pi^+\pi^-\pi^0, \tag{13}$$

$$\bar{p}p \quad \to \quad \eta\eta\pi^0, \eta \to \pi^+\pi^-\pi^0, \tag{14}$$

The remaining 373 events are attributed to reaction (8). Out of these events we find that 40 ± 5 correspond to $\bar{p}p \to \eta'\pi^+\pi^-$ with $(\eta' \to \eta\pi^0\pi^0)$ and 22 ± 3 events correspond to $\bar{p}p \to \eta'\pi^0\pi^0$ with $\eta' \to \eta\pi^+\pi^-$ (see Table 4 and figure 17).

Considering the results given in tables 2, 3 and 4 we can compare the branching ratios for reaction $\bar{p}p \to \eta'\pi^+\pi^-$ obtained from studies of reactions (6), (7) and (8). We obtain the following numbers: 0.42%, 0.39% and 0.37%, respectively. We find that these three results are in very good agreement.
We also note from Tab. 4 that the relative braching ratios for reactions $\bar{p}p \to \eta'\pi^+\pi^-$

and $\bar{p}p \to \eta'\pi^0\pi^0$ indicates that these reactions are dominated by $\eta'\sigma$ production. More precisely, we find that 33% can be attributed to $\bar{p}p \to \eta'\rho$ and 67% going into $\bar{p}p \to \eta'\sigma$.

Finally, we also note that the branching ratio for reaction (8) $(0.8 \pm 0.3)\%$ is in fair agreement with D.Urner's results $(1.39 \pm 0.36)\%$. If this reaction is dominated by the production of a σ pair, we would expect that the branching ratio for reaction (8) (first line of table 4) is equal to the branching ratio for reaction (6) (0.90 ± 0.15). This is indeed the case.

5 Amplitude Analysis

The amplitude analysis uses Nana's data and 20630 Monte Carlo events with confidence level $> 10\%$ from a 5C kinematic fit to $\eta\pi^+\pi^-\pi^+\pi^-$. The channels which are certainly required in the fit are listed below in equations (15)–(23). It is probable (and reasonable) that there is also a contribution from ${}^3S_1 \to \eta'(958)\rho$, equn.(24), though this is not cleanly separated from ${}^1S_0 \to \eta'(958)\sigma$. For present purposes, the presence of ${}^3S_1 \to \eta'(958)\rho$ does not seem controversial, so we include it:

$$
\begin{aligned}
{}^1S_0 &\to \eta(1440)\sigma;\ \eta(1440) \to \eta\sigma && (15)\\
&\to \eta(1440)\sigma;\ \eta(1440) \to a_0(980)\pi && (16)\\
&\to \eta(1800)\sigma;\ \eta(1800) \to \eta\sigma && (17)\\
&\to \eta(1800)\sigma;\ \eta(1800) \to a_0(980)\pi && (18)\\
&\to f_0(1300)\eta;\ f_0(1300) \to \sigma\sigma && (19)\\
&\to f_0(1300)\eta;\ f_0(1300) \to \rho\rho && (20)\\
&\to \eta'(958)\sigma && (21)\\
{}^3S_1 &\to [\eta(1800)\rho]_{\ell=1};\ \eta(1800) \to \eta\sigma. && (22)\\
&\to [\eta(1800)\rho]_{\ell=1};\ \eta(1800) \to a_0(980)\pi && (23)\\
&\to [\eta'(958)\rho]_{\ell=1}. && (24)
\end{aligned}
$$

Here ℓ stands for the orbital angular momentum of the final state in the production process. Also σ means the $\pi\pi$ S-wave, using the parametrisation of Zou and Bugg [8]. The $\eta(1800)$ means the very broad signal which is observed lying beneath the narrow $\eta(1440)$ in $J/\Psi \to \gamma(\eta\pi\pi)$ [9]. Present work is not sensitive to the precise mass of this resonance, which could lie anywhere within the range 1750-2100 MeV. Effectively, this channel is parametrising a broad 0^- background in $\eta\pi\pi$. The explicit form of this amplitude is given in the appendix to the technical report on Chris Pinder's data: $\eta\pi^0\pi^0\pi^0$ at rest [10].

Further channels which may plausibly be present are channels (25-27):

$$
\begin{aligned}
{}^1S_0 &\to \eta(1295)\sigma;\ \eta(1295) \to \eta\sigma && (25)\\
&\to \eta(1295)\sigma;\ \eta(1295) \to a_0(980)\pi && (26)\\
&\to a_0(1450)\pi;\ a_0(1450) \to a_0(980)\sigma. && (27)
\end{aligned}
$$

Earlier, Lucien and Nana have sought to identify $\eta(1295)$ using a procedure which selects 'symmetric' pairs of pions, section 2.4. The amplitude analysis shows that much of the signal they select in this way is actually due to $f_0(1300)$, channels (19)–(20). Nontheless, there seems to be some small remaining $\eta(1295)$ signal, which will therefore be included in the reference fit.

The $a_0(1450)$ has not been seen by VES, GAMS and E852 experiments in the $\eta\pi$ channel. This suggests it could be rather inelastic. Plausible decay modes are to $a_0(980)\sigma$ and $\rho\omega$. We search for the former in present data.

We also search for $\hat{\rho}(1405) \to f_1(1285)\pi$ or $\to B_1(1235)\pi$ in channels (28)–(31):

$$\begin{aligned}
{}^1S_0 &\to [\hat{\rho}(1405)\pi]_{\ell=1};\ \hat{\rho}(1405) \to f_1(1285)\pi && (28)\\
&\to [\hat{\rho}(1405)\pi]_{\ell=1};\ \hat{\rho}(1405) \to B_1(1235)\pi && (29)\\
{}^3S_1 &\to [\hat{\rho}(1405)\pi]_{\ell=1};\ \hat{\rho}(1405) \to f_1(1285)\pi && (30)\\
&\to [\hat{\rho}(1405)\pi]_{\ell=1};\ \hat{\rho}(1405) \to B_1(1235)\pi. && (31)
\end{aligned}$$

We find negligible contributions from all of these, but find limits on cross sections which may be useful for interpretation of other data.

Channels which we also find to be insignificant are

$$\begin{aligned}
{}^1S_0 &\to [f_1(1285)\sigma]_{\ell=1};\ f_1(1285) \to a_0(980)\pi && (32)\\
&\to [f_1(1285)\sigma]_{\ell=1};\ f_1(1285) \to \eta\sigma && (33)\\
&\to [f_1(1420)\sigma]_{\ell=1};\ f_1(1420) \to a_0(980)\pi && (34)\\
&\to [f_1(1420)\sigma]_{\ell=1};\ f_1(1420) \to \eta\sigma && (35)\\
&\to [B_1(1235)\rho]_{\ell=0};\ B_1(1235) \to \eta\rho && (36)\\
{}^3S_1 &\to [\rho'(1465)\sigma]_{\ell=0};\ \rho'(1465) \to [\eta\rho]_{\ell=1} && (37)\\
&\to [\rho'(1465)\eta]_{\ell=1};\ \rho'(1465) \to [\rho\sigma]_{\ell=0} && (38)\\
&\to [f_1(1285)\rho]_{\ell=0};\ f_1(1285) \to a_0(980)\pi && (39)\\
&\to [f_1(1285)\rho]_{\ell=0};\ f_1(1285) \to \eta\sigma && (40)\\
&\to [B_1(1235)\sigma]_{\ell=1};\ B_1(1235) \to \eta\rho. && (41)
\end{aligned}$$

These channels were considered from the outset to be unlikely, because of centrifugal barriers or high thresholds, but they were tried for completeness. Centrifugal barriers are standard Blatt-Weisskopf (Hippel-Quigg) forms with a radius of interaction of 0.8 fm.

In the amplitude analysis, four combinations of charges are required for most channels, eight for some. As an example, if we label particles $\pi_1^+\pi_2^+\pi_3^-\pi_4^-\eta$, channel 16 is described by an amplitude where labels of particles are given explicitly in parentheses:

$$\begin{aligned}
f &= BW_{1440}(135)\sigma(24)[F_{980}(15) + F_{980}(35)] && (42)\\
&+ BW_{1440}(145)\sigma(23)[F_{980}(15) + F_{980}(45)]\\
&+ BW_{1440}(235)\sigma(14)[F_{980}(25) + F_{980}(35)]\\
&+ BW_{1440}(245)\sigma(13)[F_{980}(25) + F_{980}(45)].
\end{aligned}$$

Here BW means a Breit-Wigner amplitude of constant width, σ is the parametrisation of the $\pi\pi$ S-wave, and F is the Flatté form for the $a_0(980)$, with parameters taken from the amplitude analysis of the $\eta\pi^0\pi^0$ channel, ref. [11] equns (1)–(3). As an alternative, a Breit-Wigner form for $a_0(980)$ has been tried using a mass of 985 MeV and a width of 54 MeV (Sven Ravndal's values); this gives results which are indistinguishable from the Flatté form: log likelihood differs by less than 1.

The $\eta'(958)$ has sufficient lifetime that it decays well outside the annihilation region. The long decay length randomises its phase with respect to other amplitudes. Therefore $\eta'(958)$ has been treated as incoherent with other amplitudes in the fit. Introducing interferences has almost no effect: log likelihood changes by only 2. It has been given a Gaussian line shape, with a fitted σ of 10.6 MeV in the cross section. Decays are approximated as $\eta\sigma$.

There is a strong contribution from $f_0(1300)$. In the initial discussion, we shall report results assuming a Breit-Wigner amplitude of constant width. Later, we shall discuss results obtained with a Flatté formula which includes an s-dependent width for $\rho\rho$ and $\sigma\sigma$ decays. This change has little effect on the other components in the fit, so can be considered separately.

Details of each contribution will be given in subsections below. Here we summarise results. The mass of $\eta(1440)$ optimises at 1399 MeV and the width at 46 MeV. For $\eta(1295)$ there is a weak optimum at a mass of 1255 MeV with a width of 90 MeV. The $\eta(1440)$ contributes $\sim 20\%$ of the integrated cross section and $\eta(1255)$ $\sim 3\%$. The $f_0(1300)$ will be discussed in some detail; it optimises at a mass of 1260 MeV and a width of 300 MeV.

We define the likelihood function L in the standard way so that a change of 0.5 corresponds to one standard deviation. Suppose the fitted cross section for the kinematics of a particular event is w. We define

$$S = -\ln L = N(\ln \sum_{i=1}^{M} w_i) - (\sum_{j=1}^{N} \ln w_j), \tag{43}$$

where N is the number of data events and M the number of Monte Carlo events.

In order to display the significance of each element in the fit, Table 5 summarises the change in log likelihood when each signal is omitted from the reference fit and remaining contributions are re-optimised. Tables 6 and 7 lists the percentage contributions of every channel to the integrated cross section and also the interferences between channels. Many of these interferences are large.

Fig.20 shows projections from the reference fit, channels (15)–(26). Adding further contributions has no visible effect. The projections are not fitted quite perfectly. In the $\eta\pi$ and $\pi\pi$ mass spectra there is some discrepancy at the lowest masses. These regions receive large contributions from $\eta'(958)$. It is possible that the discrepancies arise from an inadequate description of the decays of $\eta'(958)$. There is also a slight defect in fitting the 3π mass spectrum; no variation to the fit has succeeded in accounting for this discrepancy.

Channels	ΔS
$\eta(1295) \to \eta\sigma$	11.5
$\eta(1295) \to a_0(980)\pi$	0.5
Both $\eta(1295)$	32.1
$\eta(1440) \to \eta\sigma$	54.0
$\eta(1440) \to a_0(980)\pi$	36.2
Both $\eta(1440)$	72.0
$^1S_0 \to \eta(1800) \to \eta\sigma$	36.1
$^1S_0 \to \eta(1800) \to a_0(980)\pi$	18.6
Both $^1S_0 \to \eta(1800)$	82.5
$f_0(1300) \to \sigma\sigma$	61.2
$f_0(1300) \to \rho\rho$	302.1
Both $f_0(1300)$	383.0
$^1S_0 \to \eta'\sigma$	13.1
$^3S_1 \to \eta'\rho$	39.2
Both η' channels	114.7
$^3S_1 \to \eta(1800) \to \eta\sigma$	40.1
$^3S_1 \to \eta(1800) \to a_0(980)\pi$	55.8
Both $^3S_1 \to \eta(1800)$	80.4

Table 5: Changes in $S = -\log$ likelihood when channels are removed from the reference fit and remaining contributions are re-optimised.

Channel	26	25	15	16	17	18	19	20	21
26	0.1	-1.3	0.9	-0.7	-1.0	0.7	0.8	0.0	0.0
25	0.0	8.7	-13.2	8.0	18.7	-11.2	-16.8	0.6	0.0
15	-0.8	-0.3	45.3	-39.4	-86.3	46.5	46.7	2.8	0.0
16	0.6	0.3	0.1	14.6	39.8	-29.6	-19.7	-1.1	0.0
17	3.0	-22.3	17.9	-9.0	99.8	-103.1	-103.9	-2.8	0.0
18	-2.3	12.1	-7.2	5.3	0.0	34.3	-6.6	-1.0	0.0
19	-1.0	8.6	0.0	-0.6	0.0	0.2	36.0	1.2	0.0
20	0.0	-2.2	4.7	-1.2	-7.5	1.7	6.9	26.5	0.0
21	0.0	0.0	0.0	0.0	0.0	0.0	0.0	0.0	16.4

Table 6: Percentage contributions to the integrated cross section from $^1S_0$ channels, and interferences between channels. The upper off-diagonal elements show real parts of interferences and the lower off-diagonal elements the imaginary parts of interferences.

Channel	22	23	24
22	39.4	-33.2	0.0
23	0.0	13.5	0.0
24	0.0	0.0	6.2

Table 7: Percentage contributions to the integrated cross section from $^3S_1$ channels, and interferences between channels. Off-diagonal elements are as in Table 6.

5.1 $\eta'(958)$

We now comment on individual channels one by one, beginning with the η' signal, which is conspicuous in Fig. 20(b). If either $\eta'\sigma$ or $\eta'\rho$ is excluded from the fit, Table 5 shows that log likelihood changes by a much smaller amount than if both are excluded. There is obviously some cross-talk between these channels; consequently relative branching ratio between $\eta'\sigma$ and $\eta'\rho$ should be regarded as approximate. We have checked that this uncertainty has no significant repercussions on other physics conclusions. In view of the multiplicity 3 for $^3S_1$ initial states and the $\ell = 1$ centrifugal barrier for $\eta'\rho$, the relative branching fractions which are observed are entirely reasonable.

5.2 $\eta(1440)$

Fig. 21(a) shows the variation of log likelihood when the mass of $\eta(1440)$ is varied. The mass optimises at 1399 MeV, with a statistical error of ± 4 MeV. This compares with 1400–1415 MeV in Chris Pinder's data on $\eta\pi^0\pi^0\pi^0$ and 1409 ± 3 MeV quoted by David Urner [12]. However, from Table 6 it is evident that interferences with the broad background amplitudes are large, and these may well shift the fitted mass. The width will likewise be affected by coherence with the broad background. Fig. 21(b) shows that it optimises at 46 ± 6 MeV, in agreement with the value of 49 MeV obtained from Chris Pinder's data. Earlier studies of Pinder's data indicated that the mass could be shifted by ± 15 MeV by interferences with background amplitudes. Here those backgrounds seem to be under better control, but one should recognise possible systematic errors of ± 5 MeV on the mass and ± 12 MeV on the width. These estimates come from variations we have observed in fitting present data.

In Section 2.4 it was shown that asymmetric pairs of $\pi^+\pi^-$ isolate $\eta(1440)$. Figure 22 shows a comparison of the best fit with this selection procedure. There is reasonably good agreement.

Chris Pinder's data indicated large destructive interference between $\eta\sigma$ and $a_0(980)\pi$ decay modes and a branching ratio

$$r_{1440} = \frac{BR(a_0(980)\pi)}{BR(\eta\sigma)} = 0.4 \pm 0.2. \tag{44}$$

Results of the present analysis agree closely with these conclusions but are more accurate. ¿From Table 6, we find $r_{1440} = 0.32$. This result changes very little when interferences

between combinatorics are switched off. Under those circumstances, which we believe to be the correct way of evaluating branching ratios, we find $r_{1440} = 0.33 \pm 0.06(stat)$. ¿From the fluctuations we have observed when varying ingredients in the fit (e.g. dropping channels (25–26) or adding (27-41)), we assess a systematic error of $\pm 0.07(syst)$ in this ratio. The low branching ratio to $a_0(980)\pi$ is a simple and direct consequence of the small $a_0(980)$ signal in Fig. 20(a).

The Obelix group [13] has claimed the existence of a second narrow $\eta(1465)$ decaying to $[K^*(890)K]_{\ell=1}$. We have searched for it in the present data by fixing the mass of $\eta(1440)$ at 1399 MeV, inserting a second η and scanning its mass across the range 1420 to 1560 MeV. There is no indication of any optimum in log likelihood due to this second resonance.

In order to assess the statistical error (and systematic error) on r_{1440} we have adopted the following procedure. The coupling constant for $\eta(1440) \to a_0(980)\pi$ has been written in the form $(A + iB)C$, where C is the (complex) coupling constant for $\eta(1440) \to \eta\sigma$. Then A has been moved in steps across its optimum value and B and C have been optimised freely. During this procedure, the coupling constants for $\eta(1800)$ decaying to both decay channels have been fitted freely. Values of A, B, r_{1440} and log likelihood (relative to the optimum) are shown in Table X. The statistical error on r_{1440} is ± 0.064. The optimum value of r_{1440} is displaced by 0.07 from the corresponding optimum when the relative coupling constants for $\eta(1800)$ are fixed to be the same as for $\eta(1800)$. Fortuitously, this is the largest variation we have observed in r_{1440} and may be used as an estimate of the systematic error.

A + iB	log L	r_{1440}
0.07 + i0.01371	3.0	0.240
0.08 + i0.01003	0.8	0.307
0.09 + i0.00672	0.0	0.402
0.10 + i0.00546	0.7	0.474
0.11 + i0.00420	2.9	0.573

Table 8: Optimisation of r_{1440} when $\eta(1880)$ is fitted freely.

5.3 $\eta(1295)$

If this additional 0^- resonance is inserted into the analysis in the mass range 1200–1360 MeV with decay modes to both $a_0(980)\pi$ and $\eta\sigma$, there is an improvement in log likelihood of 32.1 and a significant optimum as the mass is scanned. Our earlier experience is that this magnitude of improvement in log likelihood is significant. Fig. 21(c) shows the mass scan with a width of 53 MeV (the PDG value). The mass optimises at 1255 MeV, with a statistical error of ± 9.5 MeV. Fig. 21(d) shows that the width is not very well determined. The optimum is at 90 ± 23 MeV. The best fit indicates decays almost purely

to $\eta\sigma$. However, Table 5 shows that log likelihood changes more when both are eliminated than the sum of changes when each decay mode is eliminated separately. So the fit can obviously switch amplitudes between $\eta\sigma$ and $a_0(980)\pi$ decays to some considerable extent.

The $\eta(1295)$ and $\eta(1440)$ both appear conspicuously in data from GAMS reported at Dinkelbuhl [14]. They likewise both appear conspicuously in E852 [15] and VES [16] data reported at Hadron'97. In all three experiments, there is a clear separation between 0^- and 1^+. VES and GAMS data indicate that decays of $\eta(1295)$ favour the $a_0(980)\pi$ channel over $\eta\sigma$ by about a factor 2. E852 results are less precise but suggest roughly equal branching ratios. In view of the weakness of our $\eta(1295)$ signal, we need to be cautious in any claim about the branching ratio.

In Section 2.4, it was shown that symmetric pairs of $\pi^+\pi^-$ tend to select $\eta(1295)$. Fig. 24(a) shows satisfactory agreement of the fit with data using this selection procedure. Removing $\eta(1295)$ reduces the quality of the fit somewhat, as shown in Fig. 24(b). We therefore have some qualitative evidence for the presence of $\eta(1295)$ as well as the quantitative evidence from the mass scan of Fig. 21(c).

Fig. 23 shows the projection of $\eta'(958)$, $\eta(1440)$, $\eta(1800)$ and $\eta(1295)$ on to $s(\eta\pi^+\pi^-)$ from one combination only. The $\eta(1295)$ signal is not visible as a peak, but only as a small destructive interference around $s = 1.7$ GeV^2. This does not inspire confidence in its actual presence.

The broad $\eta(1800)$ background seems rather smaller, compared to the $\eta(1800)$ peak, than in data on $J/\Psi \to \gamma(\eta\pi^+\pi^-)$ where the height of the $\eta(1440)$ peak is roughly the same as the broad background on which it sits.

The small branching ratio for production of $\eta(1295)$ compared with $\eta(1440)$ in present data is a surprise requiring some explanation. GAMS, VES and E852 data all indicate roughly equal production of $\eta(1295)$ and $\eta(1440)$. These experiments involve production from π^- beams, a process clearly involving quarks. In contrast, annihilation is potentially a glue-rich process. A conventional interpretation would be that the 0^- glueball is produced preferentially in annihilation and that $\eta(1440)$ is the glueball. However, a difficulty with this interpretation is that the decays of $\eta(1440)$ are not flavour blind: decays to $K\bar{K}\pi$ are considerably stronger than to $\eta\pi\pi$. An alternative interpretation advanced in reference [9] is that $\eta(1800)$ is the glueball and mixes with $\eta(1440)$, which is taken to be the nonet state of the radial excitation. This interpretation is consistent with the flavour blind decays observed for $\eta(1800)$. It is pointed out in ref. [9] that the glueball will mix with SU(3) singlets. So the inference from present data would be that $\eta(1295)$ is nearly an SU(3) octet state and $\eta(1440)$ is nearly an SU(3) singlet. The fact that the broad $\eta(1800)$ is not conspicious in GAMS, VES and E852 data is consistent with those data being governed by processes involving quarks.

5.4 Branching Ratios

This is a topic on which there has been considerable argument and confusion in the past. Therefore we repeat the arguments for the purposes of clarity.

We wish to determine branching ratios for production of a particular resonance, e.g. $\eta(1440)$ and its subsequent decays. Tables 6 and 7 contain interferences between combinations; these distort the resonance branching ratios. The branching ratios should be proportional to the squares of coupling constants in the fit. This makes it clear that one should eliminate interferences between different resonances in evaluating branching ratios, as argued in the paper on $5\pi^0$ at rest [19]. Our procedure is as follows. We fit the data including all interferences and normalise to the observed branching fraction of $\bar{p}p \to \eta\pi^+\pi^-\pi^+\pi^-$ namely 0.9%. This determines coupling constants absolutely. Next we switch off interferences between resonances. We now take $\eta(1440)$ as an example. There are four charge combinations. We multiply the branching ratio for one combination by a factor 4 to allow for this, but drop interferences between different combinations. This is equivalent to considering decays of each combination 'in free space', without interference with spectators. However, for one particular resonance, e.g. $\eta(1440)$, there may be significant interferences between the two decay modes, which will be present for the resonance in all circumstances, both in present data and for decays 'in free space'.

We keep this interference and evaluate its contribution to the branching ratio. Table 8 shows branching fractions evaluated in this way. Results are quoted in Table 8 for the fit decribed below which includes the s-dependence of the width of $f_0(1300)$. Values given in the Table correspond only to the charges observed in present data. Any arithmetic for other charge states needs separate consideration, particularly interferences between different decay modes of one resonance.

The phase space for production of some resonances in $\bar{p}p$ annihilation is cut off kinematically. A clear example is that of $f_0(1300)$, where the available mass range extends only up to 1330 MeV. The numbers given in Table 8 are integrated only over the available phase space.

5.5 $f_0(1300)$

Table 5 shows that this resonance makes a very large improvement (383.0) in log likelihood. Its presence is correspondingly clear in the 4π mass projection. Fig. 25 shows the projection with $f_0(1300)$ omitted from the fit. The requirement for a high mass f_0 is obvious.

We shall now argue on the basis of branching ratios to 2π and 4π that the signal in present data cannot be $f_2(1270)$ or $f_0(1500)$ or the broad resonance in the $\pi\pi$ S-wave.

The amplitude analysis of data at rest on $\eta\pi^0\pi^0$ gives in Table 3 of Ref. [18] quite a small branching ratio for $\bar{p}p \to \eta f_0(1300)$ followed by decays to $2\pi^0$, namely $0.12 \pm 0.12 \times 10^{-3}$. Allowing for $\pi^-\pi^+$ charge states, the total rate for production of $f_0(1300)$ decaying to 2π is a factor 3 larger. It is shown below that present data give a branching ratio for production of $f_0(1300)$ with subsequent decays to all 4π charge states of 1.28×10^{-2}. The conclusion is that 4π decays are a factor 30–40 stronger than 2π decays, though the error is clearly at least a factor 2. Curtis Meyer has provided us with preliminary rough estimates from $\bar{p}n \to \pi^-4\pi^0$; the branching ratio $4\pi/2\pi$ is rather similar to the factor

Channel	Branching fraction $\times 10^{-4}$
$\eta(1295) \to \eta\sigma$	0.1
$\eta(1295) \to a_0(980)\pi$	3.6
$\eta(1295)$ interference $\eta\sigma \times a_0(980)\pi$	-0.8
All $\eta(1295)$	2.9
$\eta(1440) \to \eta\sigma$	17.6
$\eta(1440) \to a_0(980)\pi$	5.7
$\eta(1440)$ interference $\eta\sigma \times a_0(980)\pi$	-14.0
All $\eta(1295)$	9.3
$^1S_0 \to \eta(1800) \to \eta\sigma$	21.3
$^1S_0 \to \eta(1800) \to a_0(980)\pi$	8.5
$\eta(1800)$ interference $\eta\sigma \times a_0(980)\pi$	-19.0
All $\eta(1800)$	10.8
$f_0(1300) \to \sigma\sigma$	27.2
$f_0(1300) \to \rho\rho$	20.2
$f_0(1300)$ interference $\sigma\sigma \times \rho\rho$	6.0
All $f_0(1300)$	53.4
$^1S_0 \to \eta'\sigma$	12.6
$^3S_1 \to \eta'\rho$	5.1
$^3S_1 \to \eta(1800) \to \eta\sigma$	36.5
$^3S_1 \to \eta(1800) \to a_0(980)\pi$	14.9
$^3S_1 \to \eta(1800)$ interference $\eta\sigma \times a_0(980)\pi$	-37.4
All $\eta(1800)$	14.0

Table 9: Branching fractions for $\bar{p}p$ annihilations to channels with the charges of present data, excluding interferences between combinatorics and between different resonances.

30–40 obtained here.

The branching fraction for production of $f_2(1270)$ in $\eta\pi^0\pi^0$ data is very small: $(2 \pm 0.8) \times 10^{-6}$ [18], presumably because of the $\ell = 2$ centrifugal barrier. The predicted rate for production of $f_2(1270)$ in $\eta(4\pi)$ is then a factor 3/7 smaller. This is a factor 10^4 smaller than the branching ratio observed here.

There have been suggestions from Stefan Resag that $f_0(1300)$ might be very broad, with a width of order 1 GeV. To check this, we have increased the width of $f_0(1300)$ to a large value, 1.3 GeV. The 4π mass distribution is then given by phase space. The resulting fit gives log likelihood worse than the reference fit by 31.2. Again this result can be confirmed from known branching ratios. The analysis of CERN-Munich data shows that this component is almost elastic up to 1330 MeV: $\Gamma(2\pi)/\Gamma(4\pi) > 5$, in complete contradiction with the branching ratio deduced here.

Thirdly, let us consider $f_0(1500)$. Here it is desirable to update some earlier published results. The re-analysis of Cern-Munich data in ref. [17] found a 2π width for $f_0(1500)$ of 60 ± 12 MeV and a total width of 132 ± 15 MeV. Decays to $K\bar{K}$, $\eta\eta$ and $\eta\eta'$ account for a width of roughly 10 MeV, leaving ~ 60 MeV for the 4π channel. This is in apparent disagreement with the determination $\Gamma(4\pi)/\Gamma(2\pi) = 3.4 \pm 0.8$ from the analysis of $5\pi^0$ data [19]. However, this discrepancy is now understood. Firstly, an improved understanding of the AX, $f_2(1565)$ leads to small changes in the analysis of Cern-Munich data. A small contribution from the AX leads to a slight reduction in $\Gamma(2\pi)$ of $f_0(1500)$ to 45 ± 12 MeV and a consequent increase in $\Gamma(4\pi)$ to 75 MeV. Note that $\Gamma(2\pi)$ and $\Gamma(4\pi)$ move in opposite directions. Secondly, in the analysis of $5\pi^0$ data it was assumed that charged decays of $\sigma\sigma$ outnumber all-neutral decays by 8:1 and would increase the branching fraction observed for all-neutral decays by a factor 9. However, interference effects of a π^+ from one σ decay with the π^- from the other σ are significantly different from interferences amongst the $4\pi^0$ in all-neutral decays. (A σ is limited to the $\pi^+\pi^-$ combination, excluding $\pi^+\pi^+$ and $\pi^-\pi^-$). A correct evaluation of these interferences by Bing Song Zou shows that charged decays will be only a factor 5.6 stronger than all-neutral decays. This reduces $\Gamma(4\pi)/\Gamma(2\pi)$ for $f_0(1500)$ to 2.04 ± 0.5, in satisfactory agreement with the latest analysis of Cern-Munich data. As concerns present data, the observed ratio $\Gamma(4\pi)/\Gamma(2\pi) \simeq 30$ is clearly completely inconsistent with the ratio 2 for $f_0(1500)$. This eliminates $f_0(1500)$ as an explanation. If $f_0(1500)$ is substituted for $f_0(1300)$ in fits to present data using PDG values of $M = 1503$ MeV, $\Gamma = 120$ MeV, log likelihood is worse by 32.3 than in the reference fit.

Our conclusion is that we have valuable confirmation of the existence of $f_0(1300)$ and its strong decays to 4π.

We shall discuss the s-dependence of the width of $f_0(1300)$ below, but for the present we discuss fits with constant width. With $\Gamma = 300$ MeV, Fig. 26 shows log likelihood versus the mass. The optimum is at 1250 MeV, with a statistical error of ± 19 MeV. Similar results are obtained with a width of 235 or 380 MeV. The values obtained by Dombrowski [20], namely $M = 1380$ MeV, $\Gamma = 360$ MeV give a fit which is worse than the reference fit by 21.4. Fig. 27 compares the fitted 4π mass projection using (a) $M = 1260$ MeV,

$\Gamma = 300$ MeV, and (b) $M = 1380$ MeV, $\Gamma = 360$ MeV, Dombrowski's values. By eye one can see that (a) is slightly better. On the other hand, the phase space cuts off at 1330 MeV in present data, and this could prejudice the determination of the mass and width. We shall comment further on this question below using an s-dependent width for $f_0(1300)$.

We now return to the branching ratios for $f_0(1300)$ decay to $\sigma\sigma$ and $\rho\rho$. For $f_0(1300) \to \sigma\sigma$, only 4 charge combinations out of a possible 9 appear in present data. For decays to $\rho\rho$ only 3 out of a possible 9 appear here. Dealing with interferences between $\sigma\sigma$ and $\rho\rho$ decay modes is a more complex problem. Let us label the particles contributing to two σ as σ_{12} and σ_{34} and correspondingly for the two ρ. Amongst these particular configurations, the only interferences between the two decay modes are those evaluated here for $\pi^+\pi^-\pi^+\pi^-$. There are no further interferences amonst these configurations because ρ does not decay to $\pi^0\pi^0$ and there are no charged σ. However, there will be interferences which involve interchange of particles between $\sigma_{12}\sigma_{34}$ or between $\rho_{12}\rho_{34}$. For example, the π^+ from one σ can and will combine with the π^- from the second σ. This is the type of calculation Bing Song Zou carried out for $5\pi^0$ data. We have not done it for the present data, since the errors do not seem to warrant it. We therefore assess the approximate branching ratio for all charge states of $f_0(1300)$ to be

$$[\frac{9}{4} \times 27.2 + 3 \times 20.2 + 6.0] \times 10^{-4} = 1.28 \times 10^{-2}. \tag{45}$$

The total widths of the resonance to $\sigma\sigma$ and $\rho\rho$ are in the ratio

$$\frac{BR(f_0(1300) \to \sigma\sigma)}{BR(f_0(1300) \to \rho\rho)} = \frac{27.2}{20.2} \times \frac{9}{12} = 1.01. \tag{46}$$

This result is in agreement with Ulrike Thoma's preliminary value.

This is, however, one place where there is a significant difference between the fit with a constant width for $f_0(1300)$ and the s-dependent width. With constant width, the branching ratio between $\sigma\sigma$ and $\rho\rho$ decreases to 0.86. The difference between these two numbers is some estimate of the systematic error.

5.6 $\eta(1800)$

This broad contribution to $\eta\sigma$ gives an improvement in log likelihood of 82.5 in $^1S_0$ annihilations and a further 80.4 in $^3S_1$ annihilations. The fit is stable with $f_0(1300)$ also in the fit. Here we find a very interesting result. We have tried fitting $\eta(1800)$ decays freely to $\eta\sigma$ and $a_0(980)\pi$. Then we have done a second fit constraining the magnitude and phase of the relative branching ratios to be the same as for $\eta(1440)$. Log likelihood changes by only 2.6 between these two fits. This change in log likelihood is barely significant for two extra fitted parameters. Therefore we conclude that the data are compatible with the coupling constants for the decays of $\eta(1440)$ and $\eta(1800)$ being the same. This is NOT true for $\eta(1295)$. There, if the relative coupling constants for the two decay modes are

constrained to be the same as for $\eta(1440)$, log likelihood increses by 15.0, which is much larger and seems significant.

In ref. [9] it was suggested that the broad $\eta(1800)$ mixes with $\eta(1440)$. Then the component in $\eta(1440)$ due to the mixing will have the same decay matrix element to $\eta\sigma$ and $a_0(980)\pi$ as for $\eta(1800)$. The observations are explained naturally if other components of $\eta(1440)$ do not have large matrix elements for decay to $\eta\sigma$ and $a_0(980)\pi$.

5.7 $a_0(1450)$

We have tried adding $a_0(1450) \to a_0(980)\pi$, channel (27), to the reference fit, but log likelihood improves only by 0.7, a negligible amount. However, $a_0(1450)\pi$ is not easily distinguished from channel (18), $\eta(1800)\sigma$, $\eta(1800) \to a_0(980)\pi$. If channels (18) and (23) are removed from the fit, Table 5 shows that $ln\ L$ gets worse by 74.4. Substituting $a_0(1450)$ instead gives a compensating improvement in lnL of 16.1 and $a_0(1450)$ then contributes an absolute branching ratio of 0.5×10^{-3} in the charge states of present data. However, in this latter case, when the mass and width are scanned, there is no sign of an optimum. So there is no evidence for the presence of $a_0(1450) \to a_0(980)\sigma$. Some rough limit on the branching ratio for this mode is obtained by correcting for other charges. This brings the cross section up to a possible $(9/4) \times 0.5 \times 10^{-3} = 1.1 \times 10^{-2}$ of all annihilations. This compares with $a_0(1450)\pi \to \eta\pi\pi$ of 0.6×10^{-3}, including all charges. So present data only limit the ratio $[a_0(1450) \to a_0(980)\sigma]/[a_0(1450) \to \eta\pi]$ to ~ 2.

5.8 $\hat{\rho}(1405)$

Adding any of channels (28)–(31) to the fit gives negligible improvement in log likelihood. Values are shown in Table 10 below. It is nonthelesss useful to try to establish upper limit on the contributions these channels might make. These limits may be useful in discussing the possibility that the $\hat{\rho}(1405)$ is really a cusp due to the opening of $f_1(1285)\pi$ or $B_1(1235)\pi$ channels. We have therefore determined the magnitudes of contributions from these channels giving rise to an increase in log likelihood of 2. This corresponds statistically to a 2 standard deviation effect. Results are given in Table 9.

Channel	Fraction of present data (%)
28: $^1S_0 \to \hat{\rho}(1405)\pi,\ \hat{\rho} \to f_1(1285)\pi$	0.29
29: $^1S_0 \to \hat{\rho}(1405)\pi,\ \hat{\rho} \to B_1(1235)\pi$	0.39
30: $^3S_1 \to \hat{\rho}(1405)\pi,\ \hat{\rho} \to f_1(1285)\pi$	0.20
31: $^3S_1 \to \hat{\rho}(1405)\pi,\ \hat{\rho} \to B_1(1235)\pi$	1.03

Table 10: Contributions to present datafrom $\hat{\rho}$ giving rise to a worsening of log likelihood by 2.0.

5.9 Other channels

Remaining channels (32)–(41) have been tried in the fit, but none gives a significant improvement. This is not surprising in view of their high thresholds or centrifugal barriers. Magnitudes of observed improvements are listed in Table 10. None of these changes seems significant in view of the extra parameters, and there are no visible changes in the projections. Also, if the masses of the resonances are scanned, there is no optimum.

Channel	ΔS
28: $^1S_0 \to \hat{\rho}(1405)\pi,\ \hat{\rho} \to f_1(1285)\pi$	0.9
29: $^1S_0 \to \hat{\rho}(1405)\pi,\ \hat{\rho} \to B_1(1235)\pi$	0.4
30: $^3S_1 \to \hat{\rho}(1405)\pi,\ \hat{\rho} \to f_1(1285)\pi$	0.2
31: $^3S_1 \to \hat{\rho}(1405)\pi,\ \hat{\rho} \to B_1(1235)\pi$	1.3
32 and 33: $[f_1(1285)\sigma]_{\ell=1}$	9.8
34 and 35: $[f_1(1420)\sigma]_{\ell=1}$	9.5
36: $B_1(1235)\rho$	0.6
37: $[\rho'(1465)\eta]_{\ell=1};\ \ \rho'(1465) \to [\eta\rho]_{\ell=1}$	10.4
38: $[\rho'(1465)\eta]_{\ell=1}\ ;\ \ \rho'(1465) \to [\rho\sigma]_{\ell=0}$	14.7
39 and 40: $[f_1(1285)\rho]_{\ell=0}$	8.4.
41: $B_1(1235)\sigma$	10.7

Table 11: Changes in $S = -$ log likelihood when channels (28)–(41) are added to the reference fit.

5.10 s-dependence of $f_0(1300)$

It is obvious that $f_0(1300)$ decays much more strongly to 4π than to $\pi\pi$ and $K\bar{K}$. However, the phase space for the 4π channel is strongly s-dependent. This s-dependence is illustrated in Fig. 28 using equn. 40 from ref. [17], and including a form factor $\alpha = 1$ GeV^2 which reproduces the Vandermeulen form factor closely.

We have fitted the present data using a Flatté form

$$f = \frac{1}{[s - m^2 + iM(\Gamma_{\pi\pi}(s) + \Gamma_{KK}(s) + \Gamma_{\eta\eta}(s) + \Gamma_{\rho\rho}(s) + \Gamma_{\sigma\sigma}(s))]} \quad (47)$$

$$\Gamma_{\rho\rho}(s) = g_1 \frac{\rho_{\rho\rho}(s)}{\rho_{\rho\rho(s_0)}} \quad (48)$$

$$\Gamma_{\sigma\sigma}(s) = g_2 \frac{\rho_{\sigma\sigma}(s)}{\rho_{\sigma\sigma(s_0)}}. \quad (49)$$

The latter equations express the fact that it is convenient to normalise widths at a value of s close to the resonance peak. We choose $s_0 = 1.3^2$ GeV^2. We take $g_1/g_2 = 1.01$, as determined above. We take $\Gamma_{\pi\pi} = \Gamma_{KK} = 28$ MeV and $\Gamma_{\eta\eta} = 4.2$ MeV at $s = s_0$ from the coupled channel analysis of ref. [21], but results are not sensitive to these precise values since the 4π width dominates.

We have fitted the data with a variety of 4π widths. What we find is that the peak in 2π and $K\bar{K}$ channels is always about 75 MeV lower than in the 4π channel. This is because the rapidly increasing 4π width contributes to the denominator of the Flatté form and depresses the upper side of the resonance strongly. Secondly, we find that the full width is similar in all channels. Ulrike Thoma has given preliminary values for the mass and width in the 4π channel of 1380 MeV and 320 MeV respectively. For purposes of illustration we adopt as a compromise a peak mass of 1285 MeV in the $\pi\pi$ channel and therefore 1355 MeV in 4π, and a width of 320 MeV. Fig. 29 then illustrates the line shape of $f_0(1300)$ in the $\pi\pi$ channel (full line), the 4π channel (dotted), and in 4π as it will appear modified by the phase space available in $\bar{p}p$ annihilation at rest (dash-dotted). In the calculation of this last curve, the cross section for 4π is multiplied by $q/2M$, where q is the momentum with which $f_0(1300)$ is produced in $\bar{p}p$ annihilation. The dashed curve uses a simple Breit-Wigner amplitude of constant width with a mass of 1285 MeV. Compared with a Breit-Wigner amplitude, the upper side of $f_0(1300)$ in the 2π channel is depressed by the rising $\Gamma_{4\pi}$.

Table 11 illustrates some fits to present data. The optimum fit gives a peak position of 1255 MeV, in agreement with fits using a constant width. For these parameters, the full width at half maximum of the resonance peak is 266 MeV. The pole position is at 1255 - i123 MeV. We have tried increasing the 4π width. What happens is that the fitted peak position then moves down in mass, as shown in Table 11. Such low masses seem implausible. It is not possible to obtain a reasonable fit with the mass of the pole increased to $\sim$ 1380 MeV, as obtained by others. This is because of the suppression of the upper side of the resonance by the rapidly rising 4π cross section. It therefore seems inescapable that the peak of $f_0(1300)$ in $\pi\pi$ and $K\bar{K}$ data will lie in the range 1250-1310 MeV.

M	$\Gamma_{4\pi} = g_1 + g_2$	Peak	Half-height	full width	ΔS
1.390	0.280	1.260	1.115-1.359	0.244	1.9
1.402	0.315	1.254	1.098-1.356	0.258	0.5
1.407	0.350	1.255	1.083-1.349	0.266	0.0
1.410	0.370	1.240	1.074-1.346	0.272	0.1
1.415	0.400	1.235	1.062-1.341	0.279	0.3
1.430	0.450	1.226	1.041-1.336	0.295	0.7

Table 12: A variety of fits with s-dependent width for $f_0(1300)$. Masses are in GeV.

We remark that data on $\bar{p}p \to \eta K\bar{K}$ would be valuable for estimating the branching ratio of $f_0(1300)$ to $K\bar{K}$. This channel should be free of $f_2(1270)$ and $a_2(1320)$ and should be rather simple to analyse.

5.11 Summary

The essential points which have emerged from this analysis are as follows:

- The $\eta(1440)$ is definitely present, but with large interferences with $\eta(1800)$; the value of r_{1440} is in agreement with that determined from Chris Pinder's data and is 0.33 ± 0.06, where the error covers systematic variations.
- The $\eta(1295)$ appears to be present with a small branching fraction of $\sim 2.9\%$ of present data, but with a mass of 1255 ± 9.5 MeV, and poorly determined width.
- The $\eta(1800)$ has the same relative coupling constants to $a_0(980)\pi$ and $\eta\sigma$ as $\eta(1440)$, in both magnitude and phase.
- The $f_0(1300)$ is confirmed; when fitted with a Flatté formula including the s-dependence of $\Gamma_{\rho\rho}$ and $\Gamma_{\sigma\sigma}$, the pole position is at $M = 1257 - i124$ MeV from present data.
- Some upper limits are established on the presence of $\hat{\rho}$ and $a_0(1450)$.

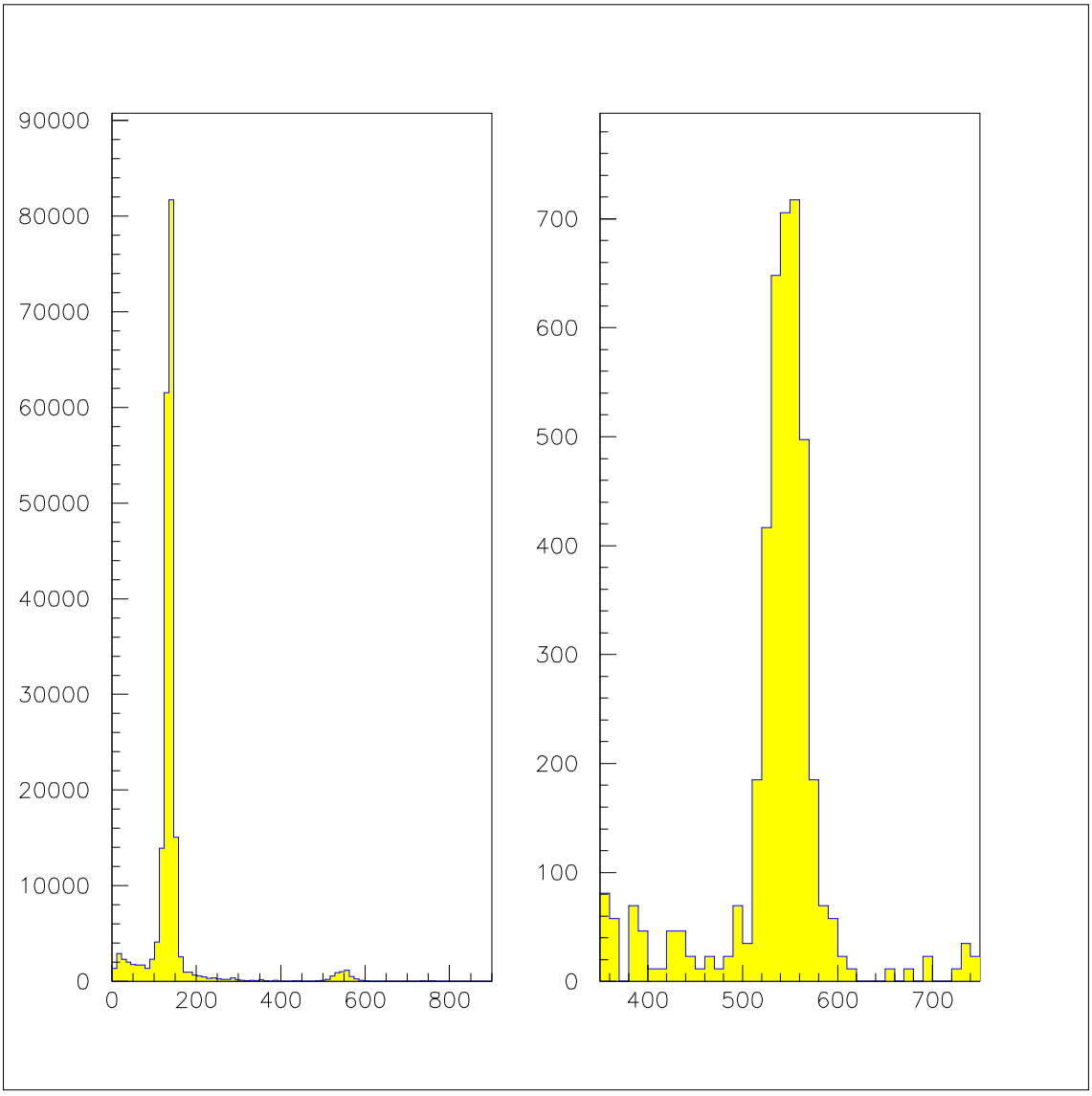

Figure 1: *$\gamma\gamma$ invariant mass distribution for 208K events after 10% CL cut on hypothesis* $2\pi^+2\pi^-2\gamma$.

6 Figures

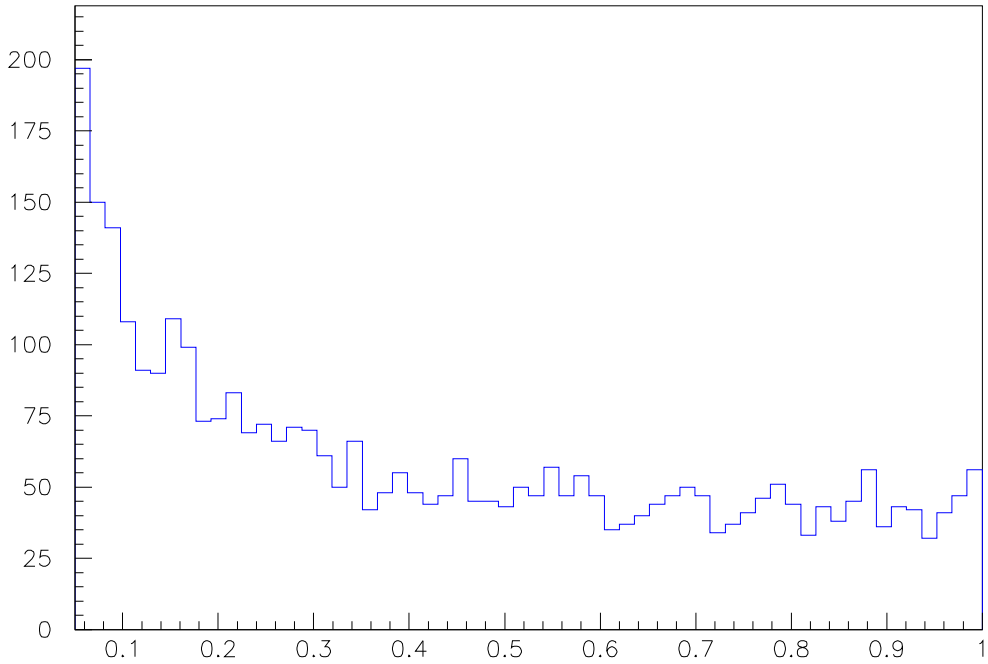

Figure 2: *CL distribution for the* $2\pi^+2\pi^-\eta$ *hypothesis.*

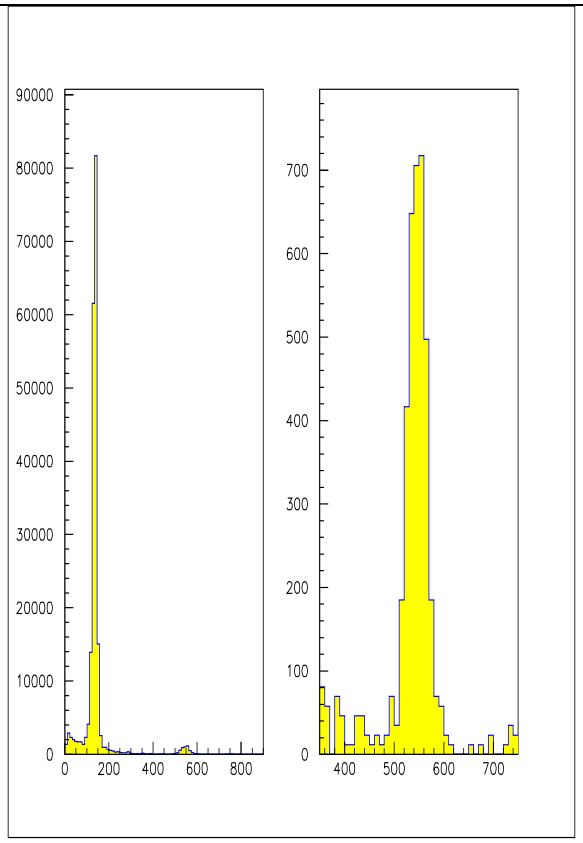
90000
80000
70000
60000
50000
40000
30000
20000
10000
0
0 200 400 600 800
700
600
500
400
300
200
100
0
400 500 600 700

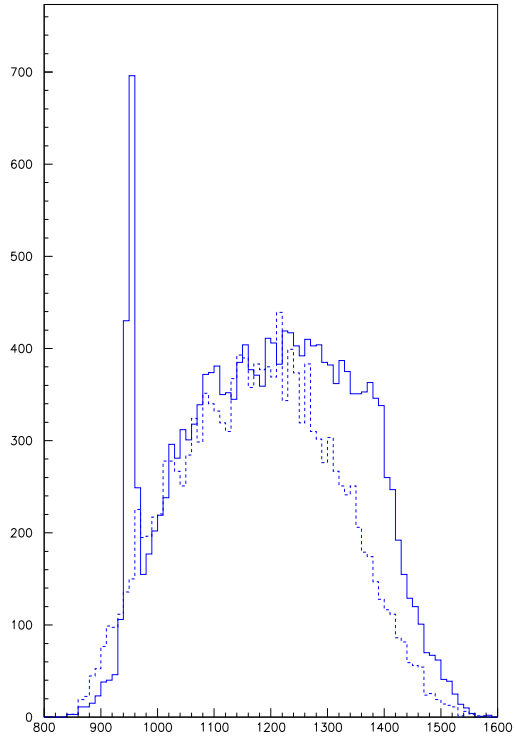
700
600
500
400
300
200
100
0
800 900 1000 1100 1200 1300 1400 1500 1600

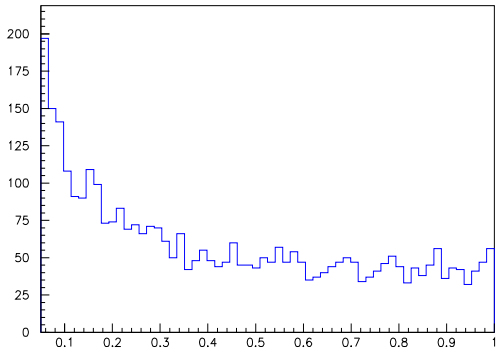
200
175
150
125
100
75
50
25
0
0.1 0.2 0.3 0.4 0.5 0.6 0.7 0.8 0.9 1

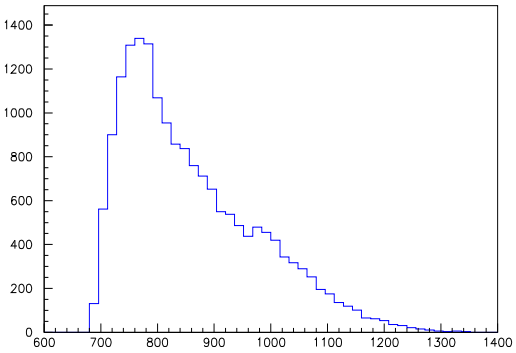
1400
1200
1000
800
600
400
200
0
600 700 800 900 1000 1100 1200 1300 1400

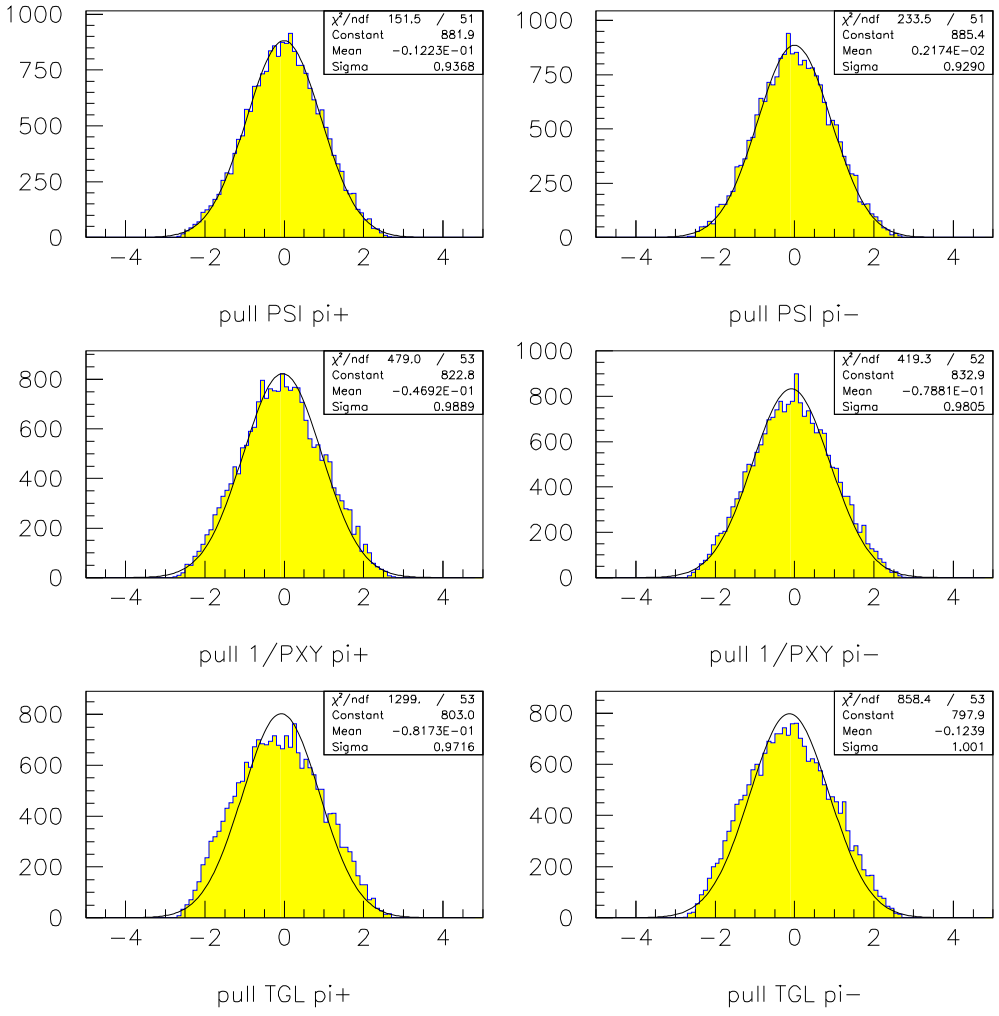

Figure 3: *Pulls from the kinematic fit to the hypothesis* $2\pi^+2\pi^-\eta$.

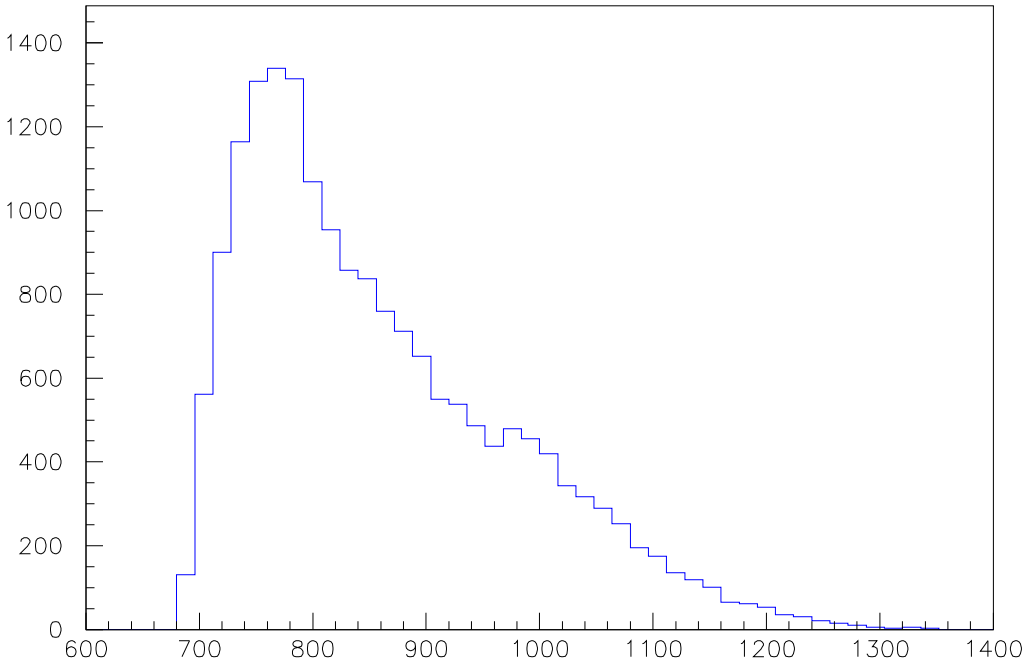

Figure 4: *The $\eta\pi^{\pm}$ effective mass distribution.*

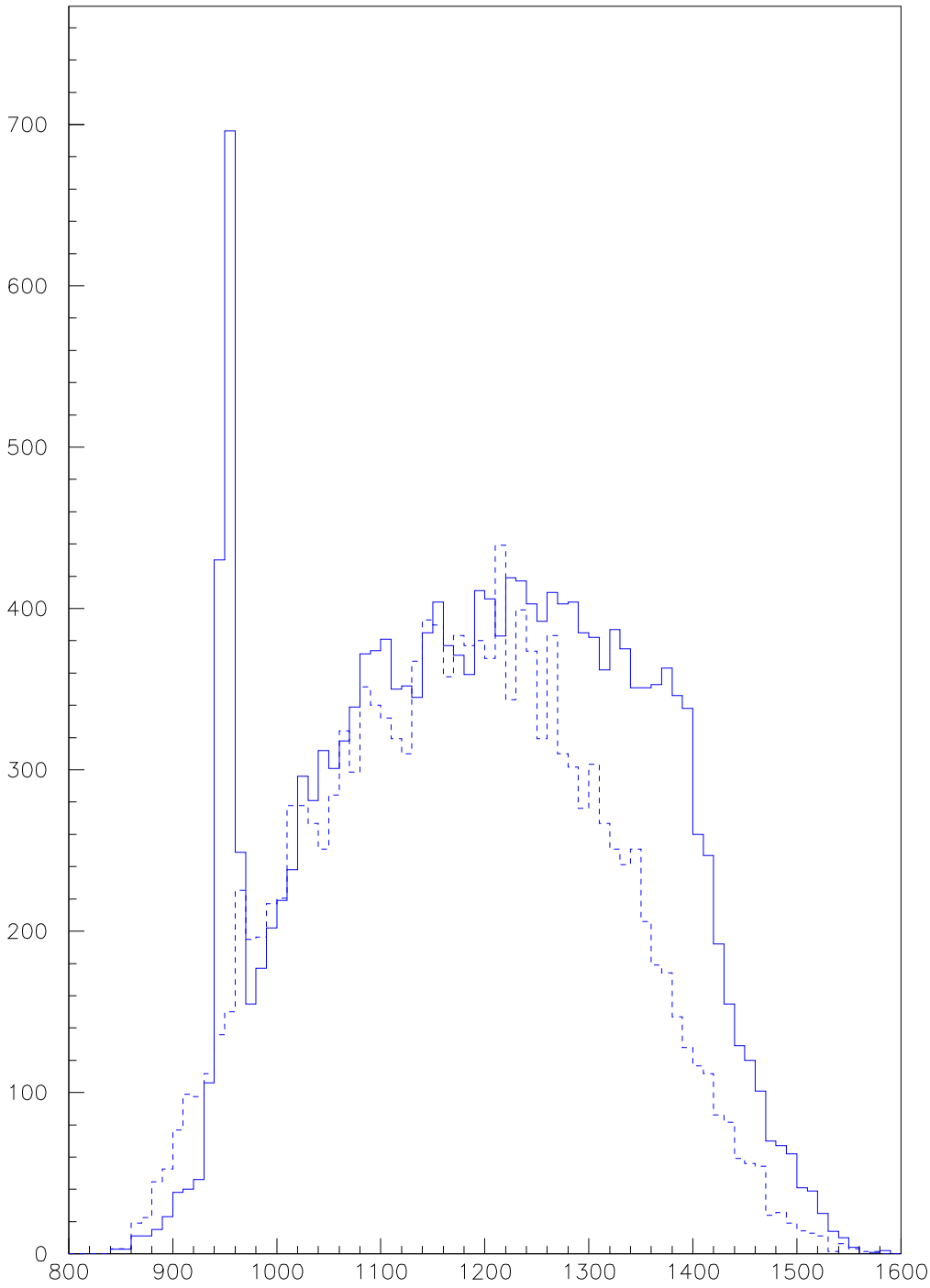

Figure 5: *The $\eta\pi\pi^-$ (light grey) and $\eta\pi^-\pi^-$, $\eta\pi^+\pi^+$ effective mass distributions.*

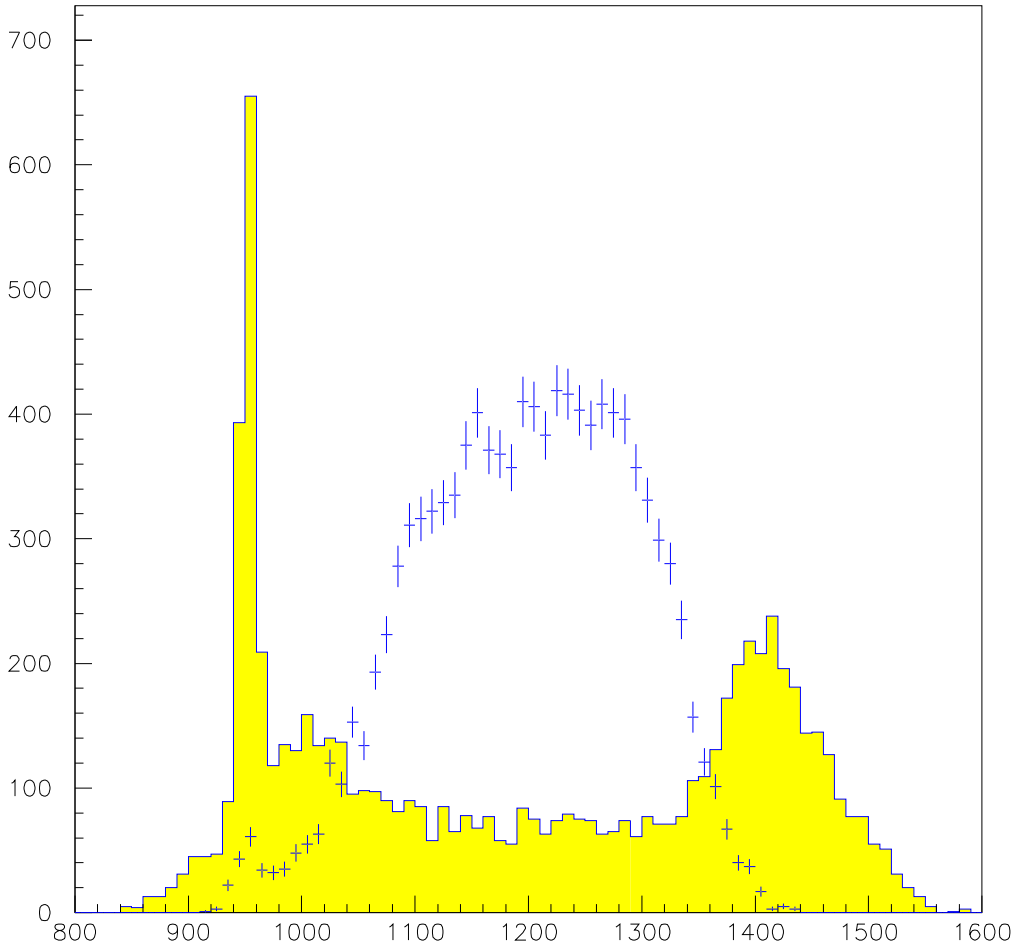

Figure 6: *The $\eta\pi^+\pi^-$ invariant mass distribution for asymmetric events (histogram) and for symmetric events (crosses) for the value of $\alpha = 0.6$.*

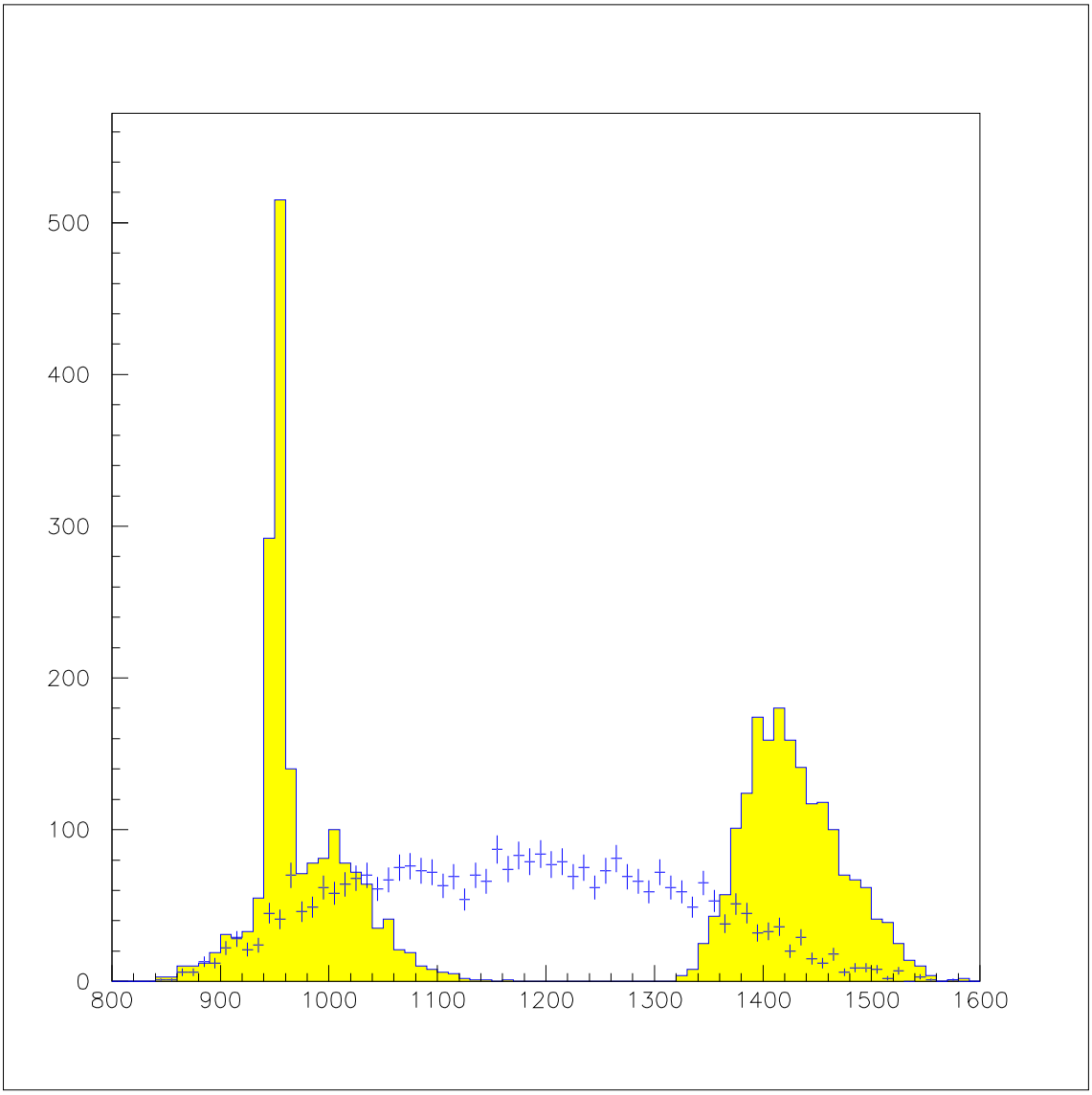

Figure 7: *The $\eta\pi^+\pi^-$ invariant mass distribution for the non-crossing combinations for the asymmetric events.*

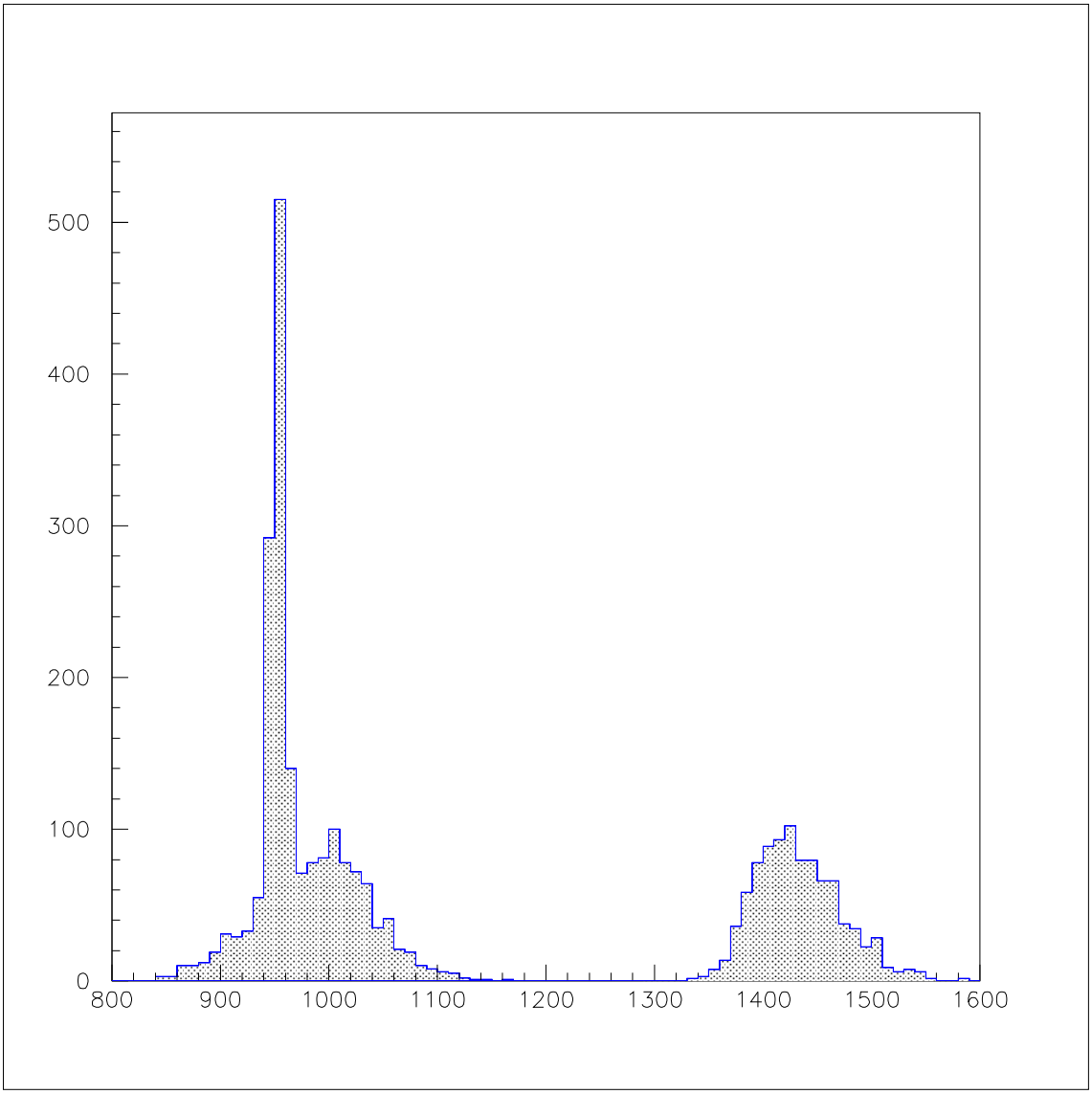

Figure 8: *The $\eta\pi^+\pi^-$ invariant mass distribution without η' reflection in the E/ι region.*

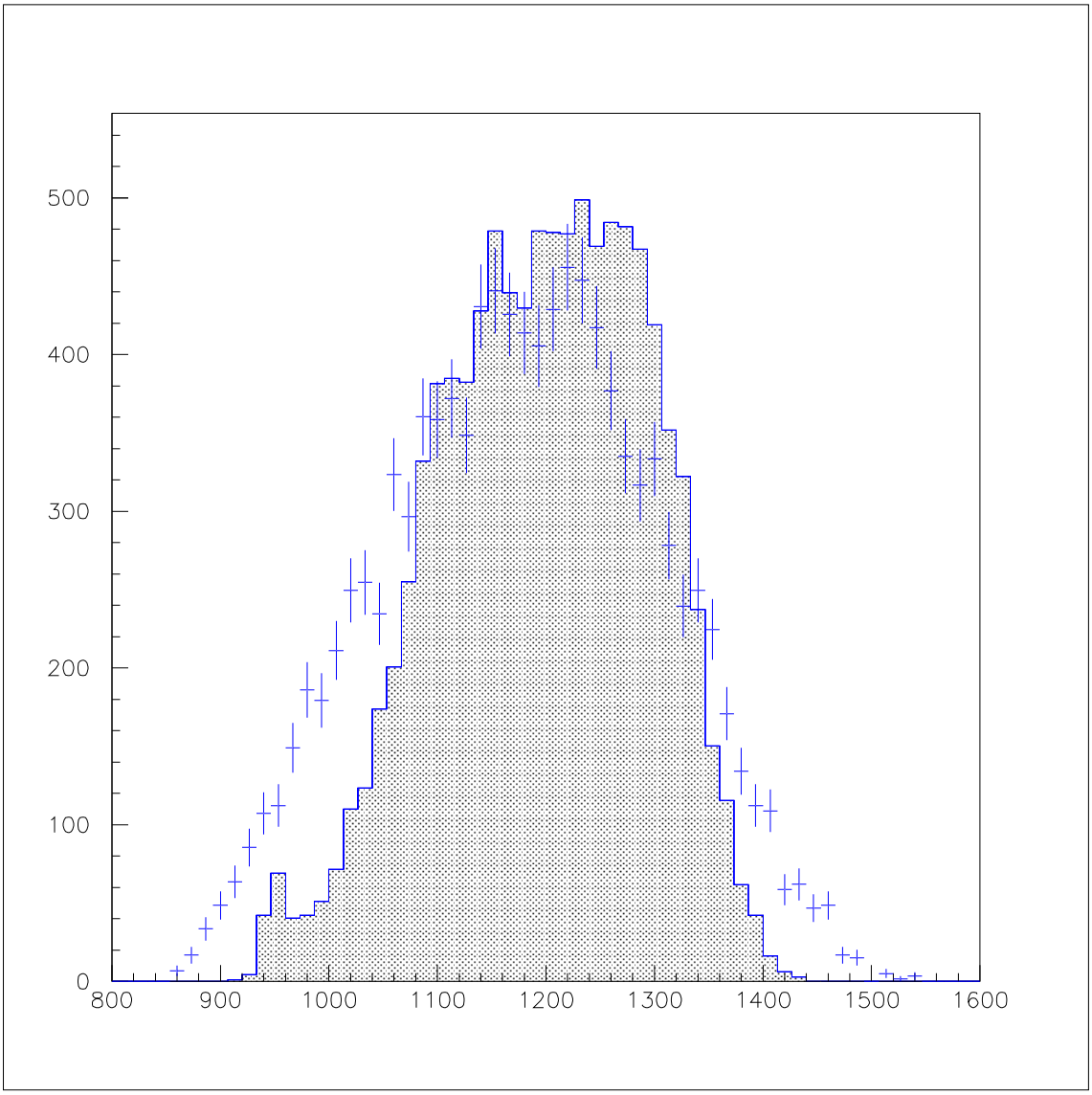

Figure 9: *The $\eta\pi^+\pi^-$ invariant mass distribution for symmetric events: histogram represents the data, whereas crosses the 'phase space' MC.*

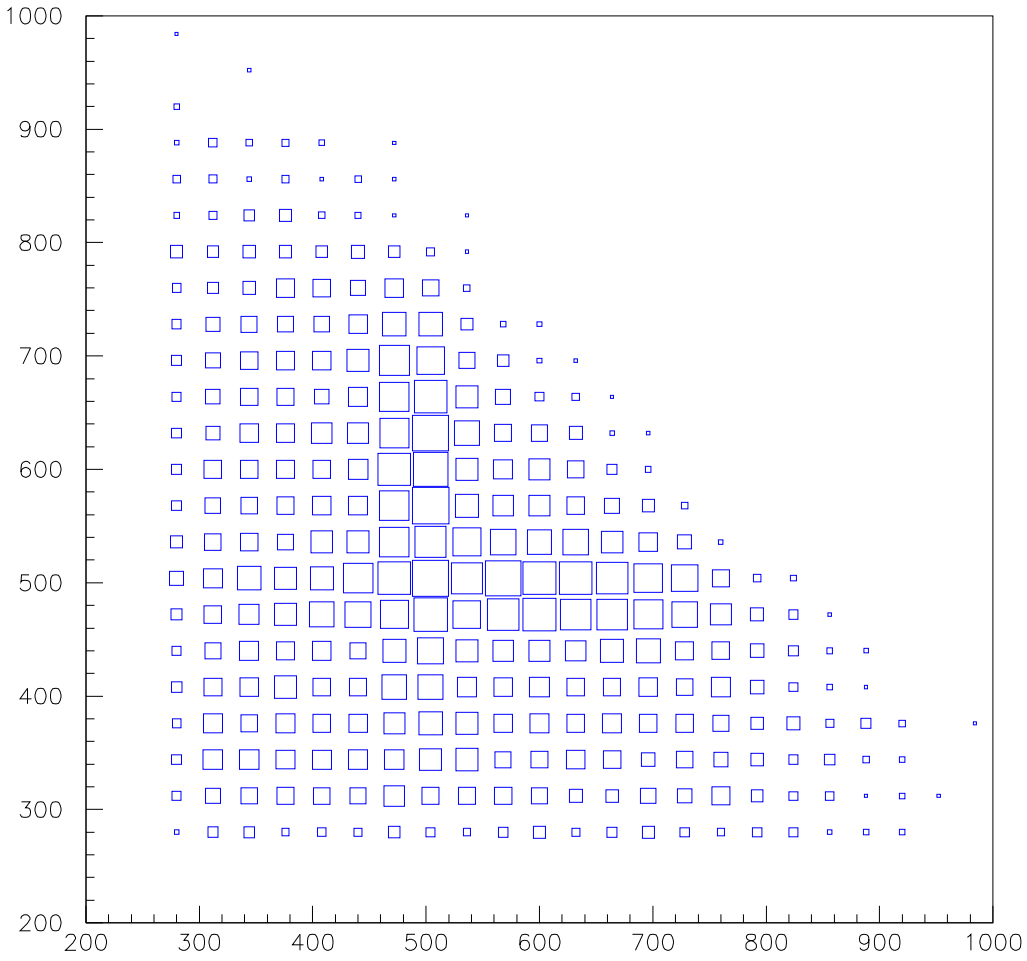

Figure 10: *The scatter plot* $m(\pi^+\pi^-)$ *versus* $m(\pi^+\pi^-)$ *for symmetric events (data).*

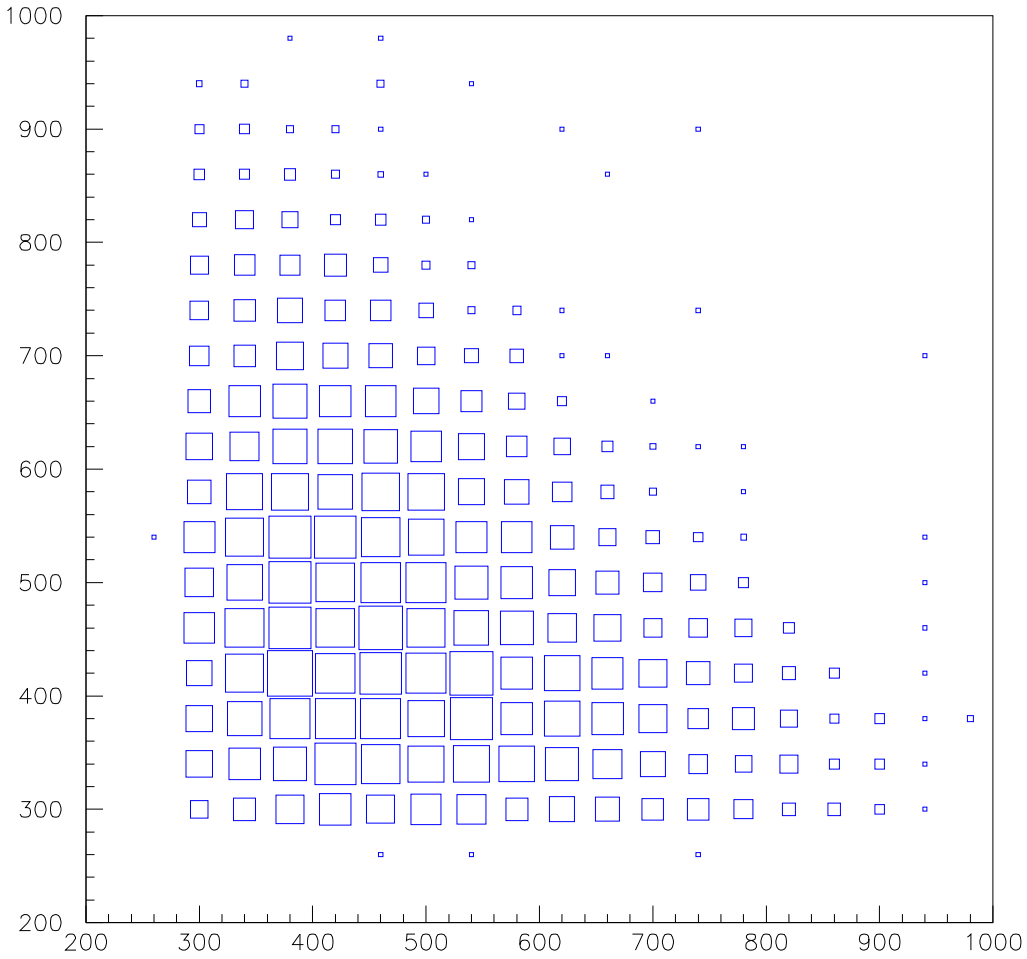

Figure 11: *The scatter plot $m(\pi^+\pi^-)$ versus $m(\pi^+\pi^-)$ for symmetric events (MC phase space).*

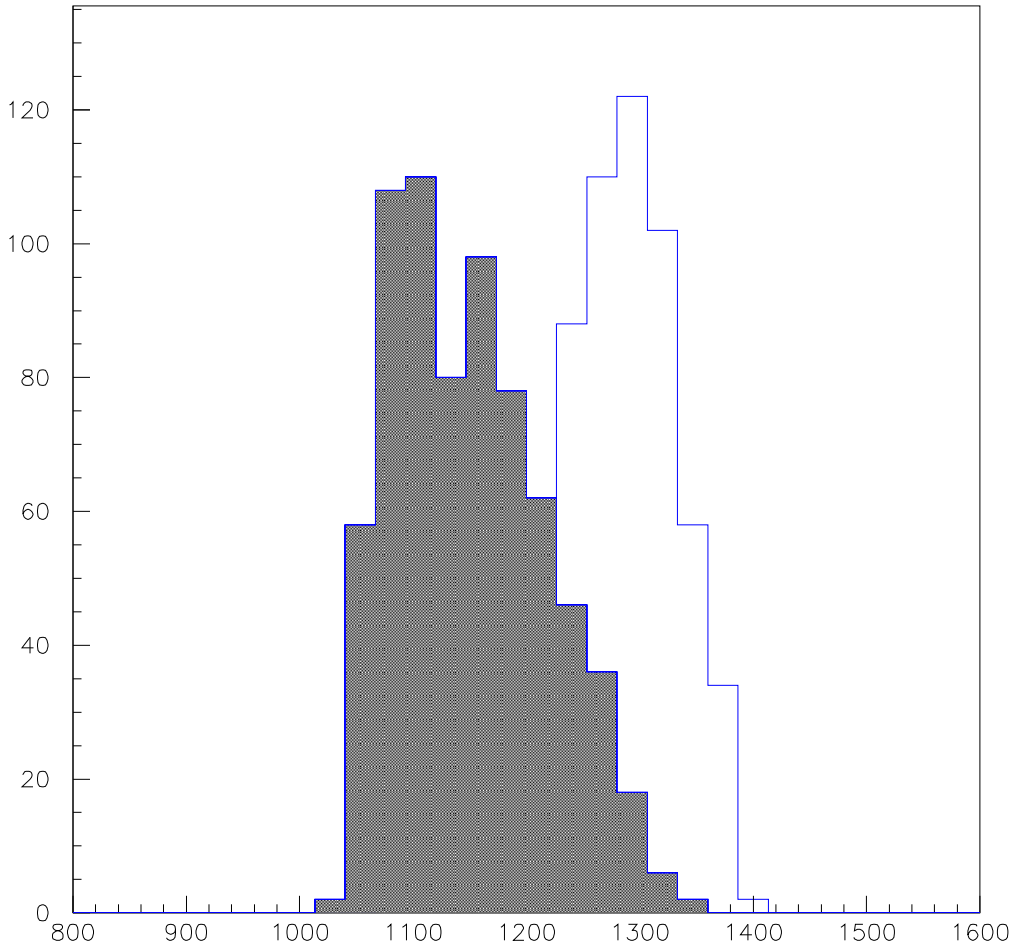

Figure 12: *The $\eta\pi^+\pi^-$ mass distribution (for details see text).*

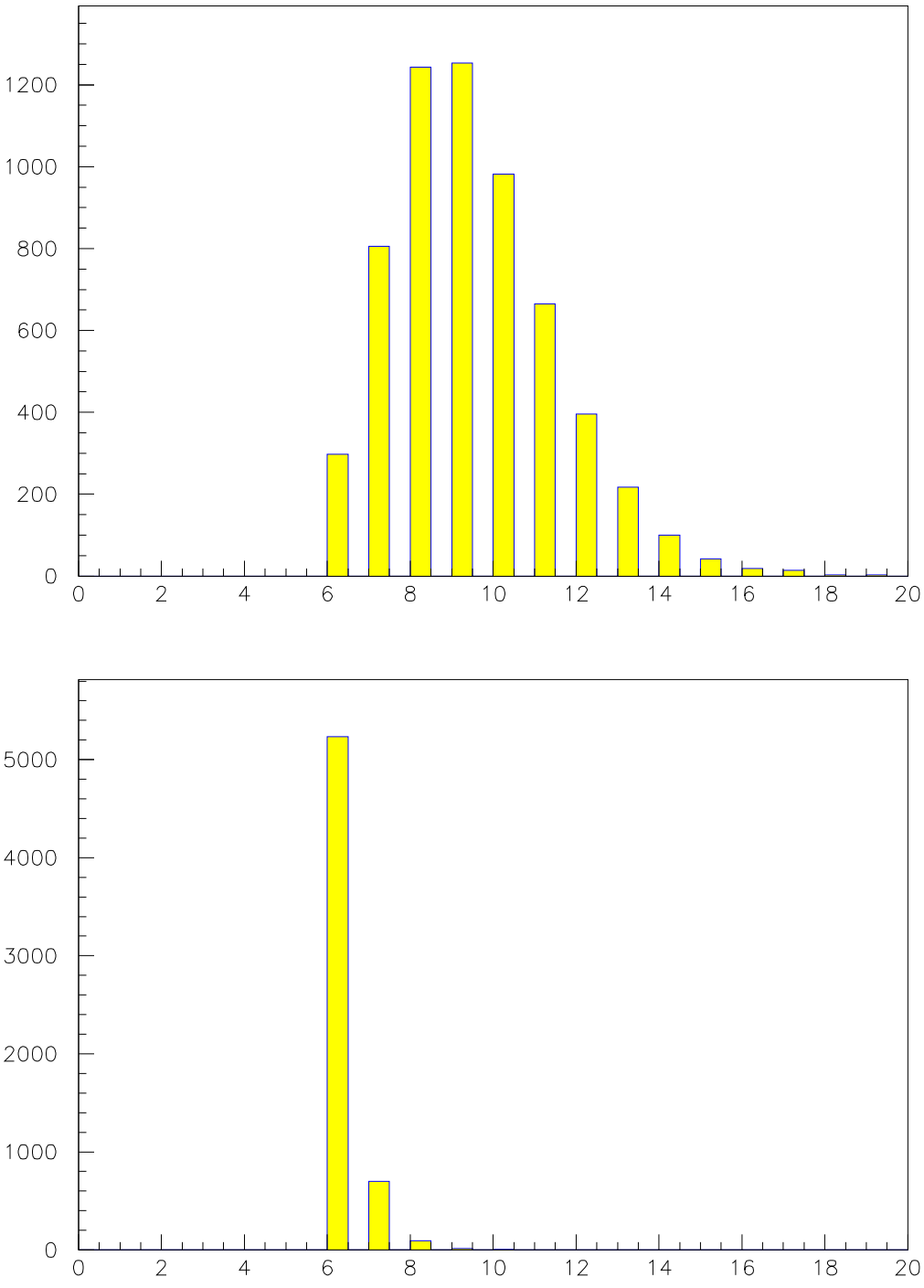

Figure 13: *The PED and γ^* distributions for the 6040 events which fit the reaction* $\bar{p}p \rightarrow 2\pi^+2\pi^-3\pi^0$.

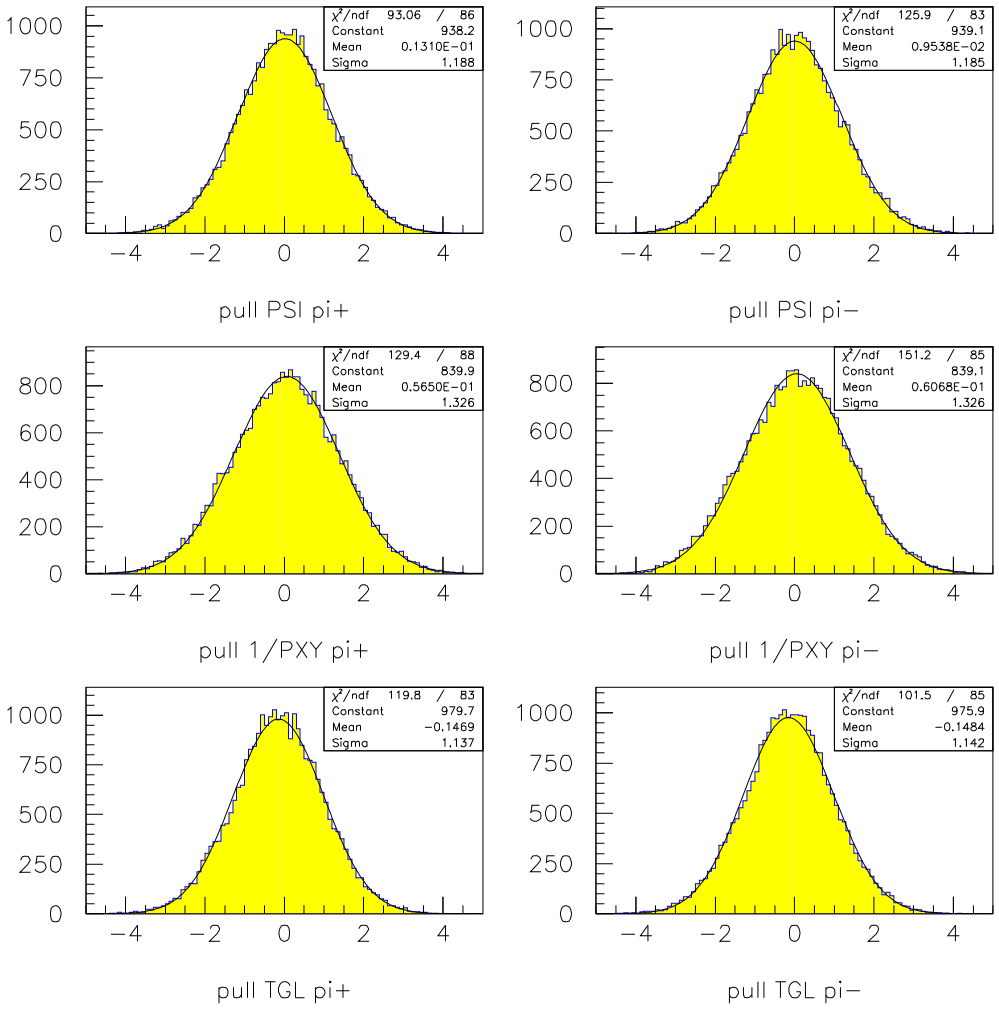

Figure 14: *Pulls from the kinematic fit for the reaction* $2\pi^+2\pi^-3\pi^0$.

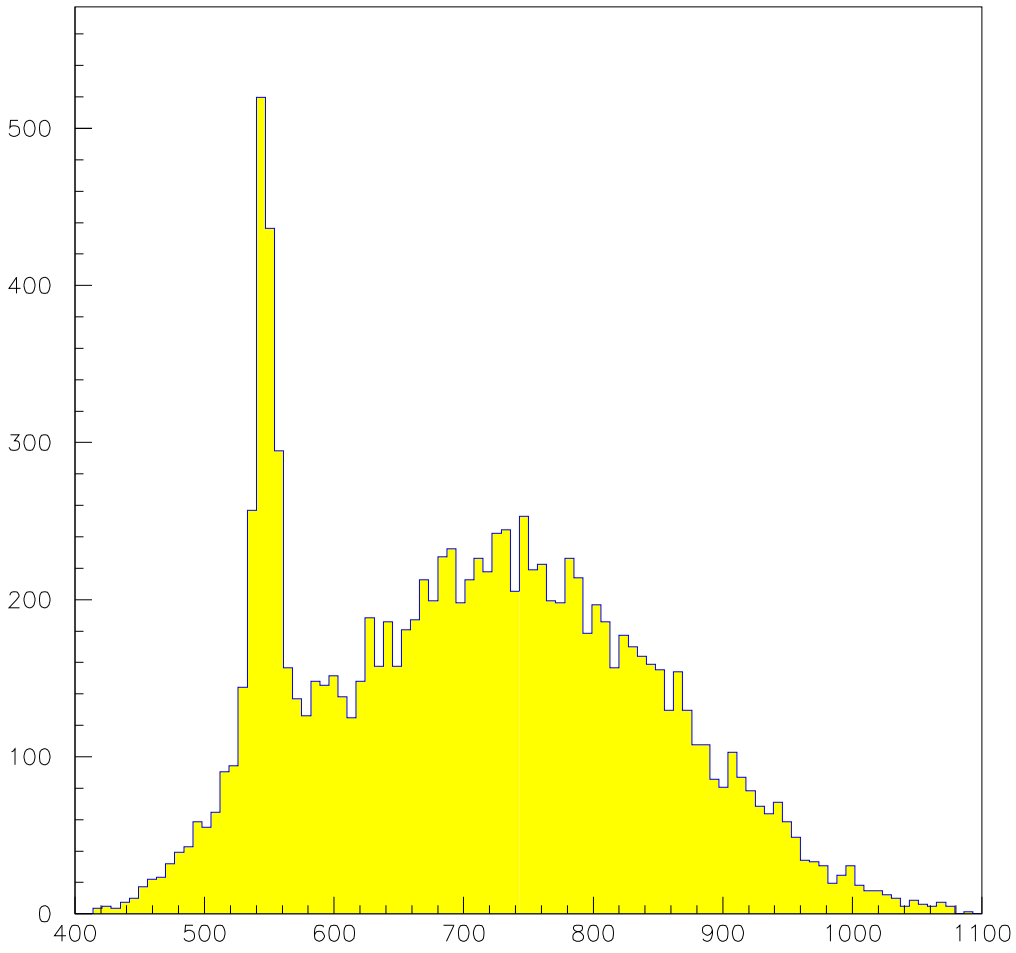

Figure 15: *The* $3\pi^0$ *invariant mass distribution.*

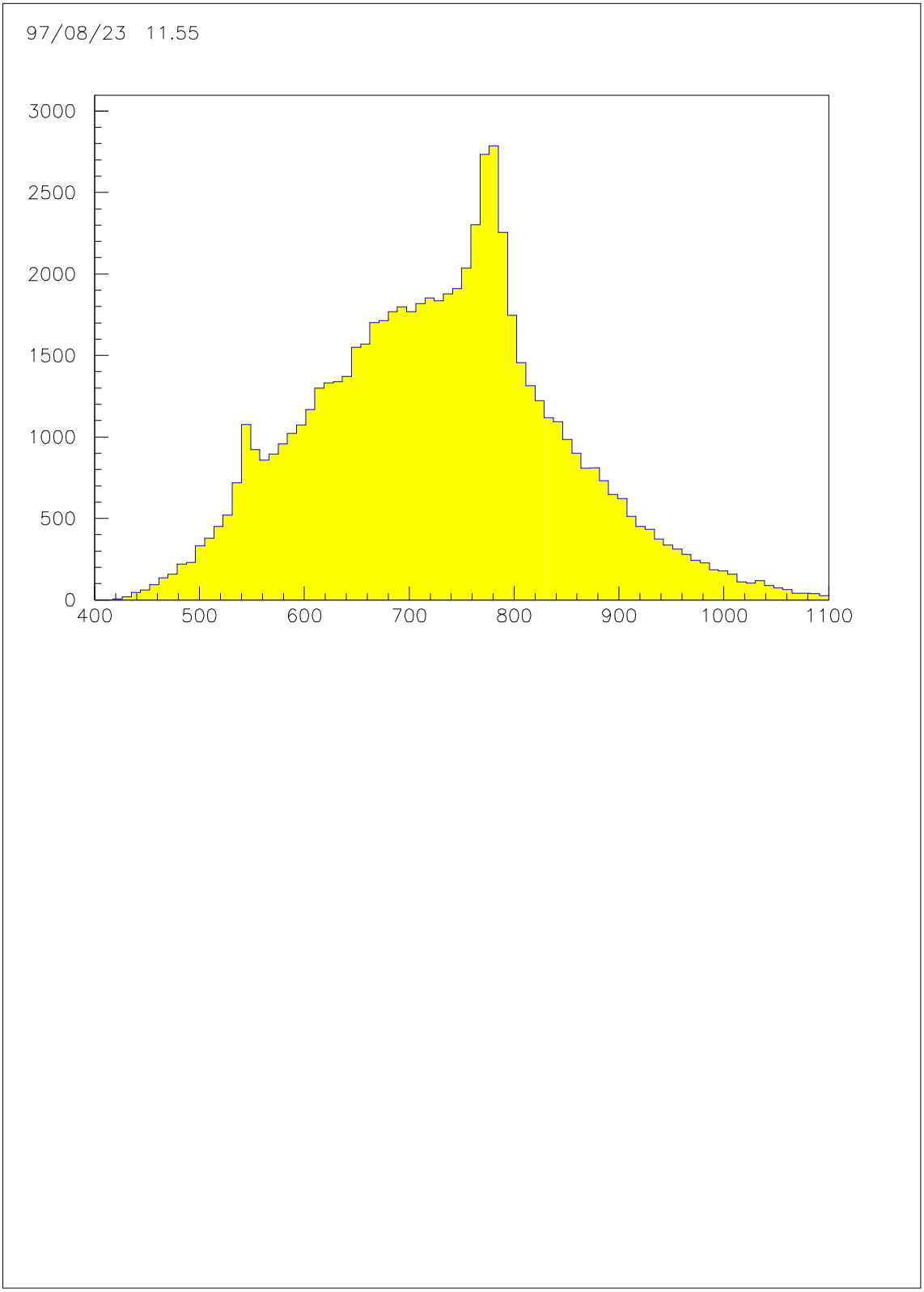

Figure 16: *The $\pi^+\pi^-\pi^0$ invariant mass distribution.*

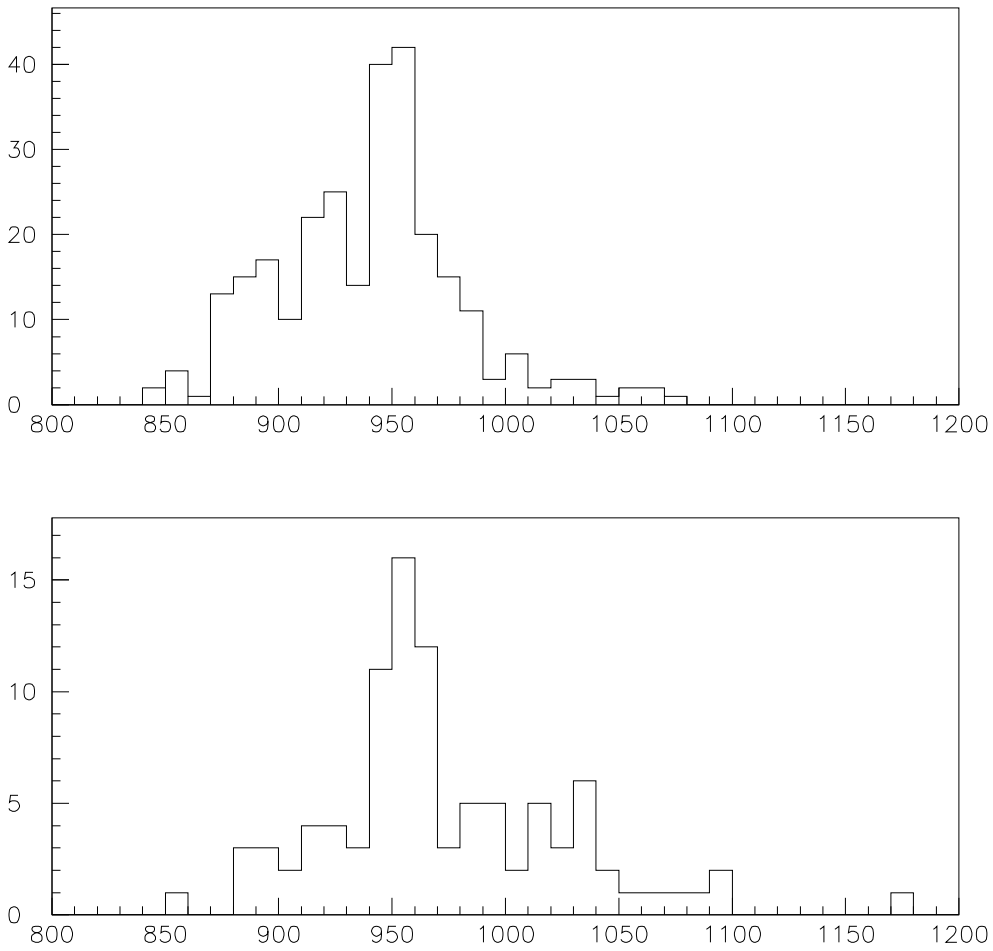

Figure 17: *The $\eta\pi^+\pi^-$ (up) and $\eta\pi^0\pi^0$ (down) invariant mass distributions.*

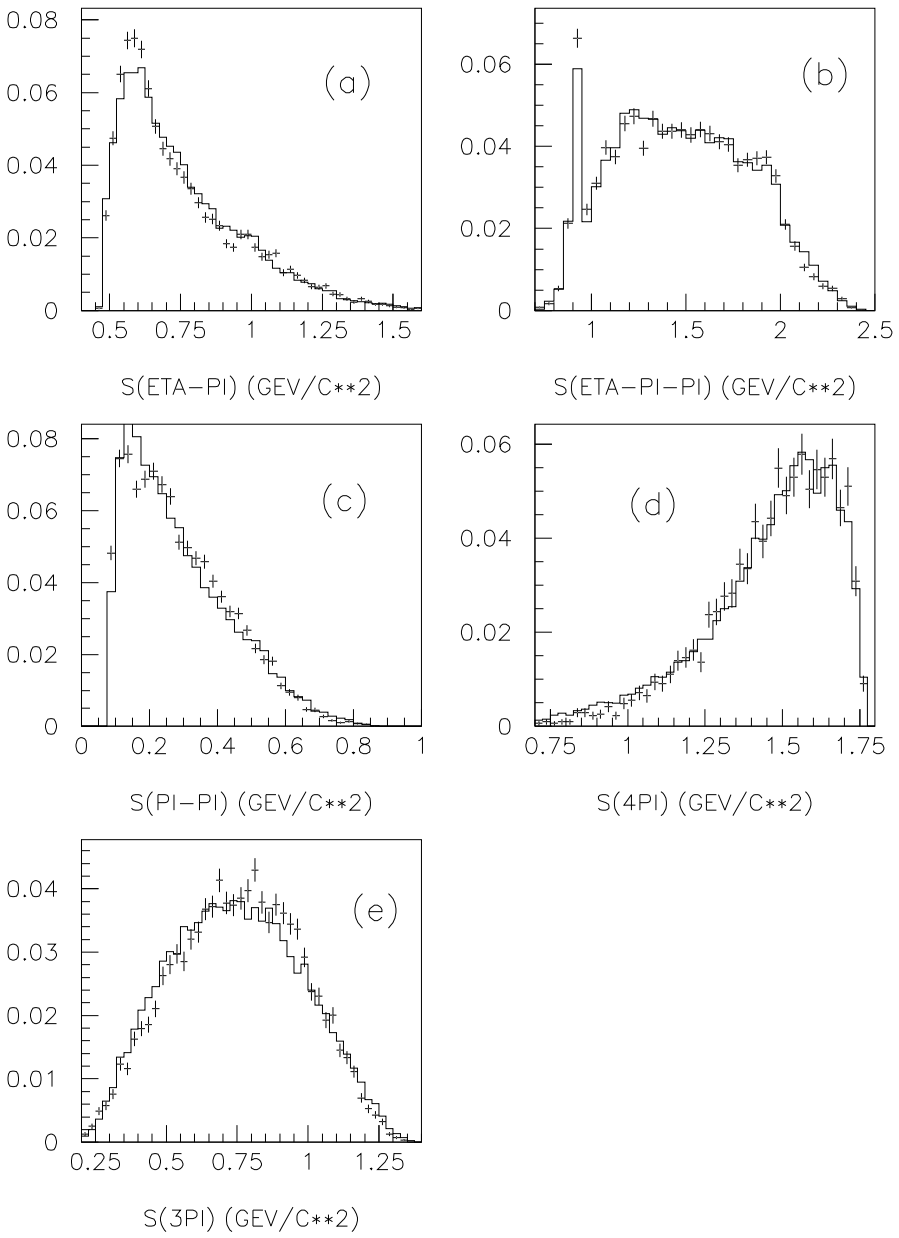

Figure 18: *Projections on to (a) $s(\eta\pi)$, (b) $s(\eta\pi^+\pi^-)$, (c) $s(\pi^+\pi^-)$, (d) $s(4\pi)$, and (e) $s(3\pi)$. Histograms show the fit..*

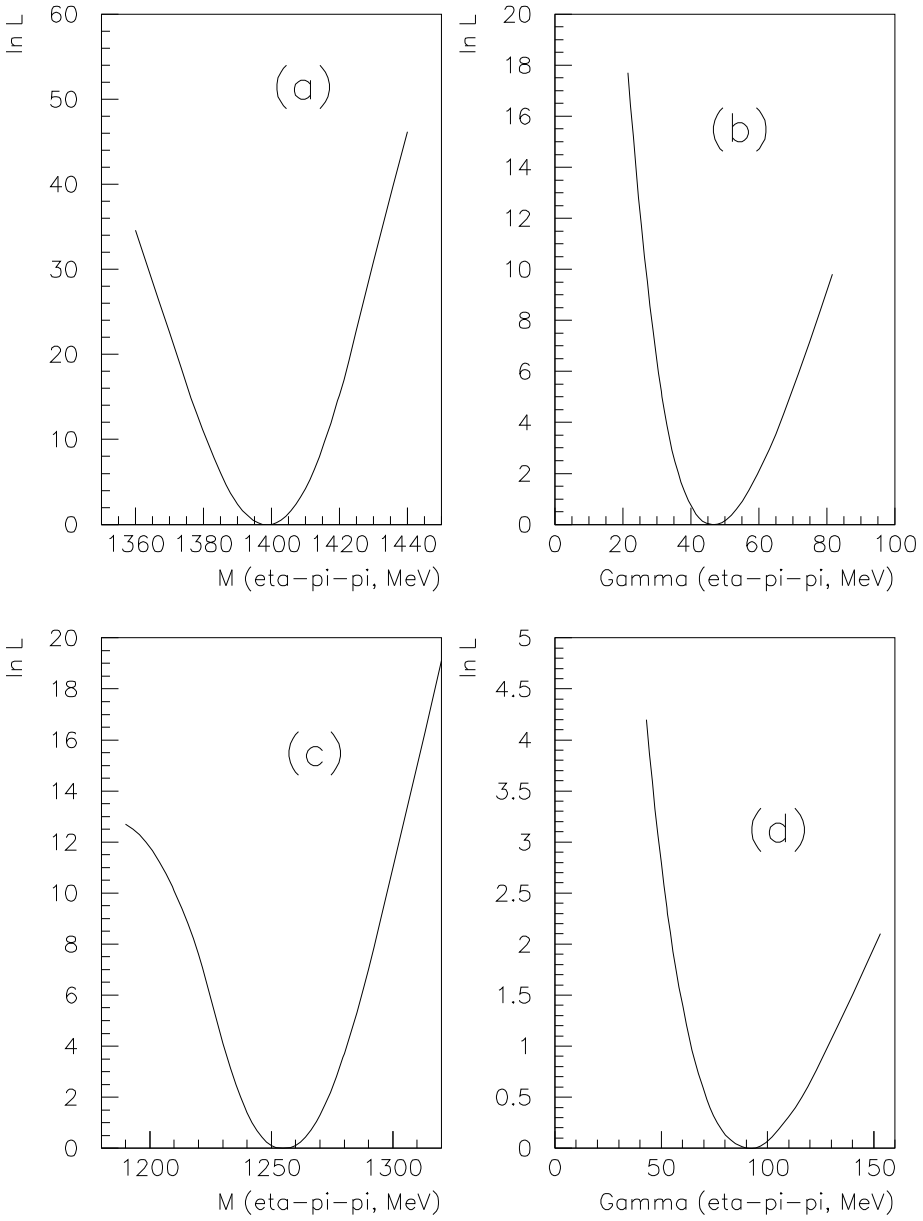

Figure 19: *Log likelihood v. (a)* $M(\eta(1440))$*, (b)* $\Gamma(\eta(1440))$*, (c)* $M(\eta(1295))$*, and (d)* $\Gamma(\eta(1295))$.

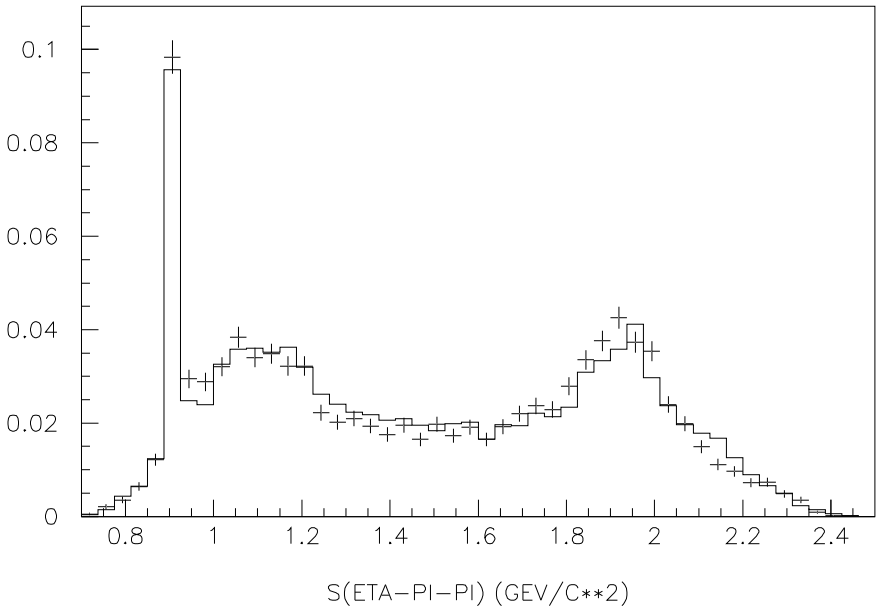

Figure 20: *Comparison of the best fit with asymmetric pairs of pions, as defined by equns. (12).*

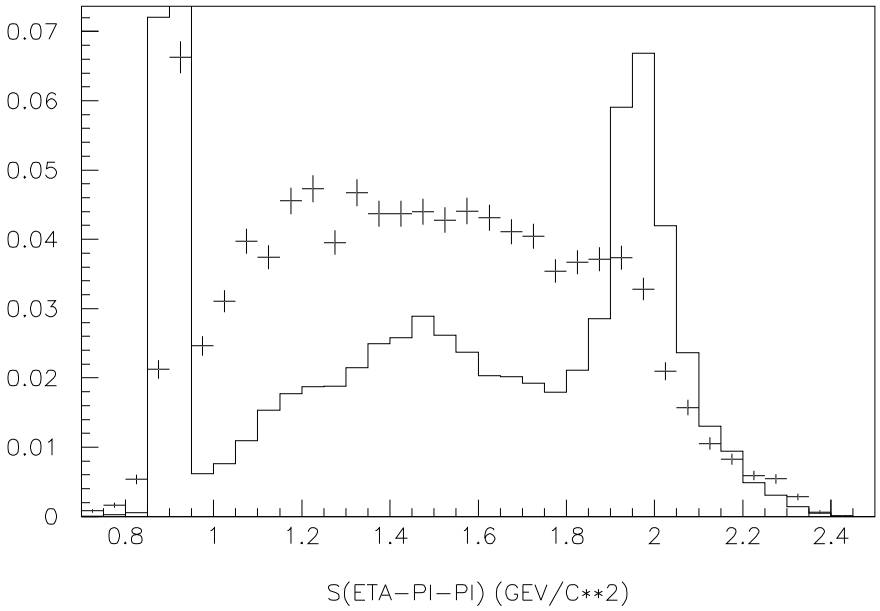

Figure 21: *Projection on to* $s(\eta\pi^+\pi^-)$ *from one combination of* $\eta'(958)$, $\eta(1295)$, $\eta(1440)$ *and* $\eta(1800)$.

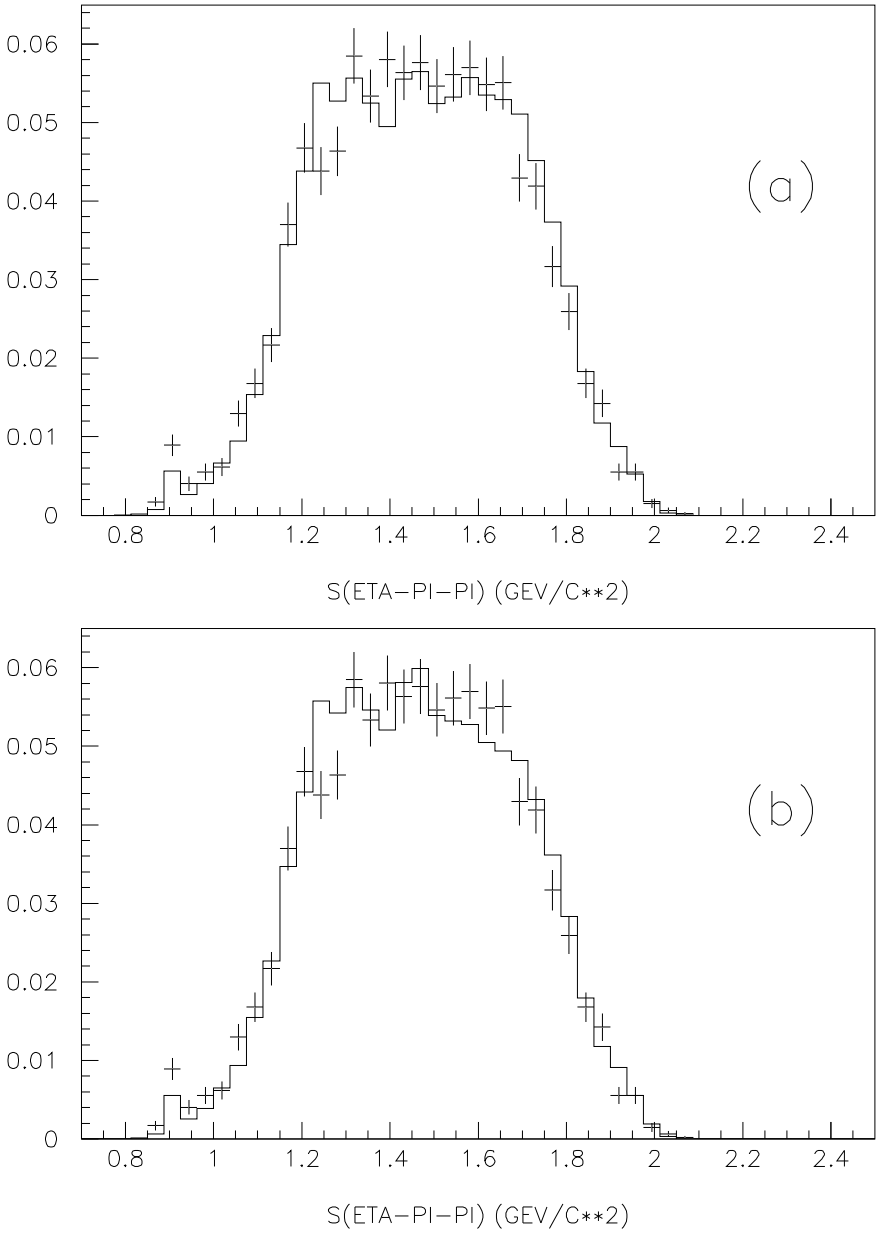

Figure 22: *Comparison with (a) symmetric pairs, (b) symmetric pairs when* $\eta(1295)$ *is omitted.*

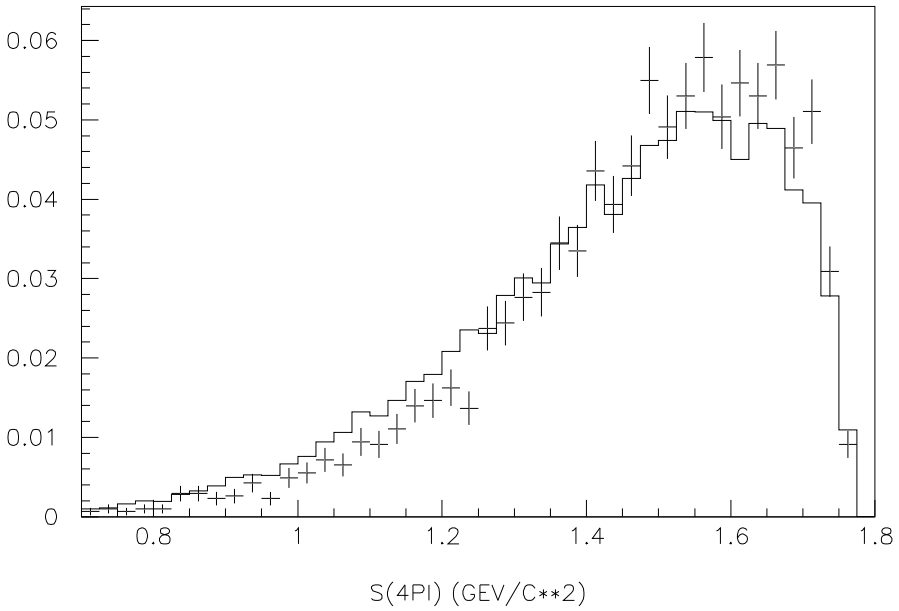

Figure 23: *Projection on to* $s(4\pi)$ *when* $f_0(1300)$ *is omitted.*

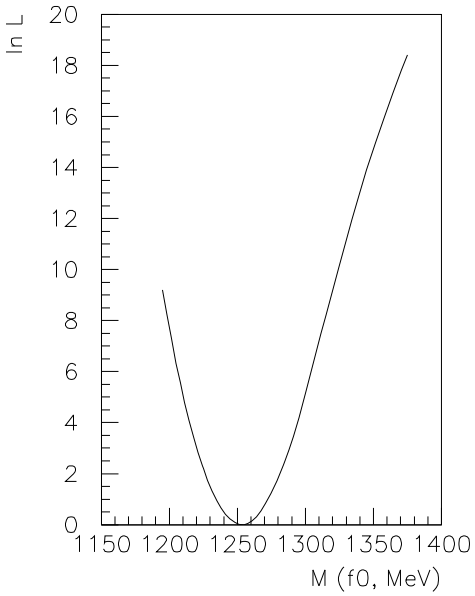

Figure 24: *Log likelihood v. the mass of* $f_0(1300)$.

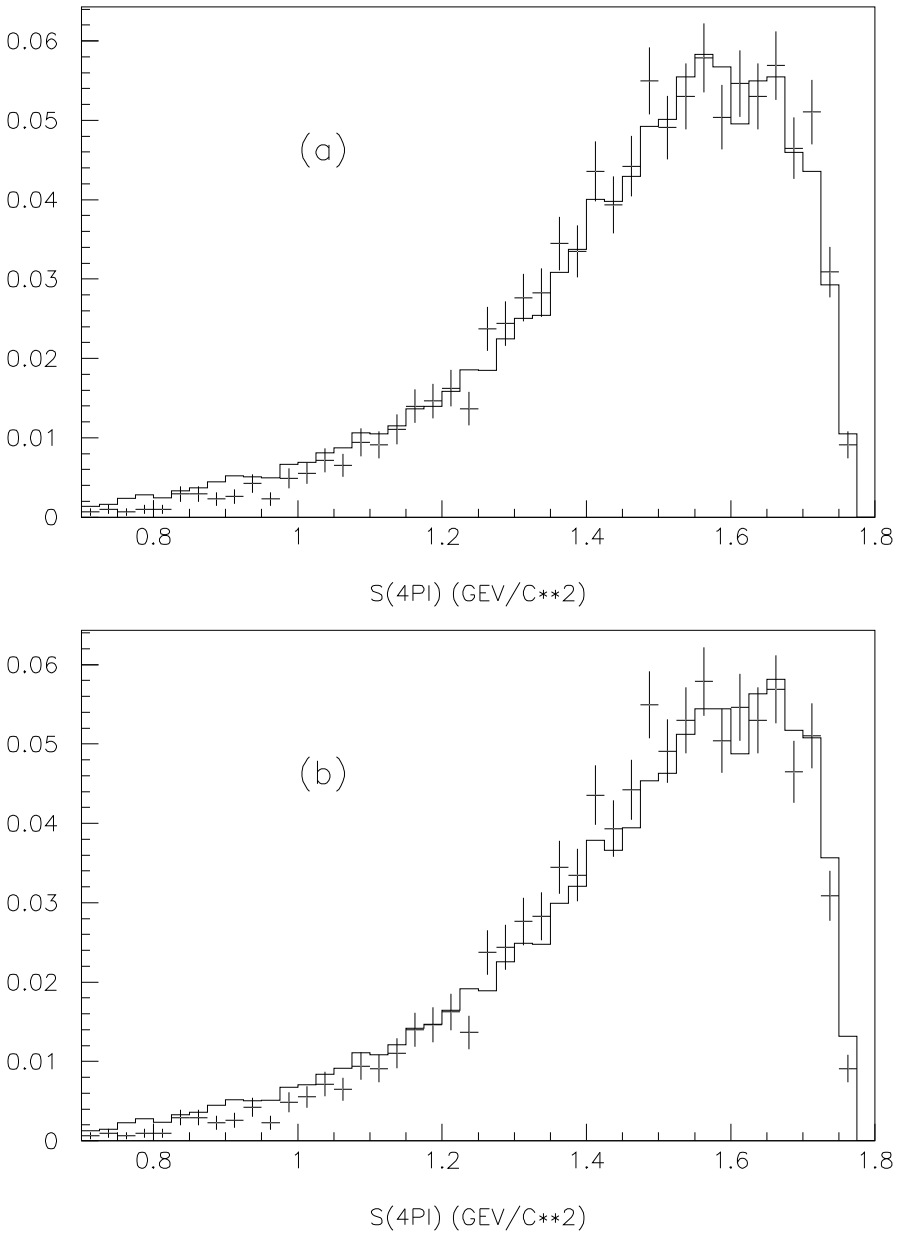

Figure 25: *Projection on to $s(4\pi)$ (a) from the reference fit, (b) using for $f_0(1300)$ Dombrowski's values $M = 1380$ MeV, $\Gamma = 360$ MeV.*

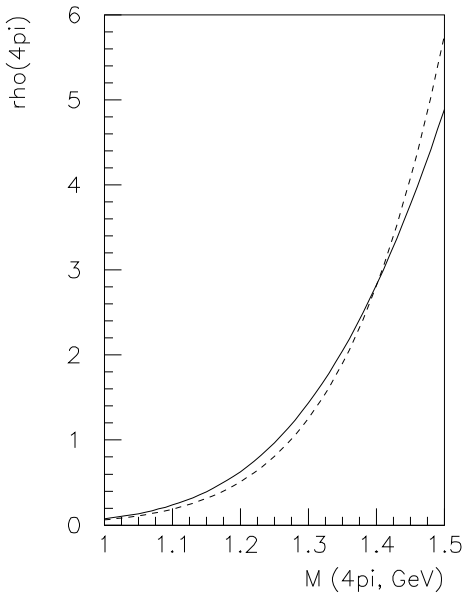

Figure 26: *The mass dependence of $\sigma\sigma$ (full curve) and $\rho\rho$ (dashed) phase space, assuming a Vandermeulen form factor.*

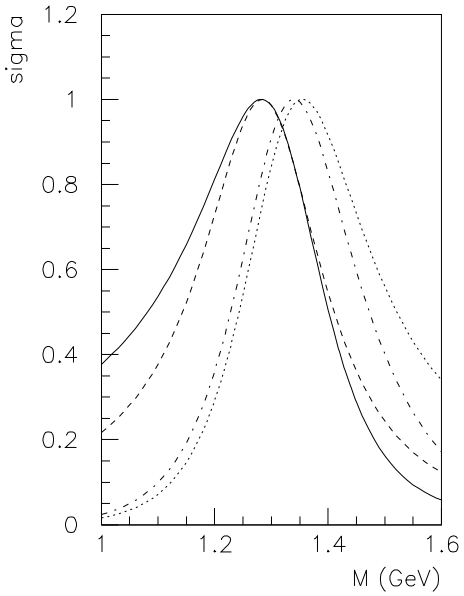

Figure 27: *The cross section for $f_0(1300) \to \pi\pi$ (full curve) compared with a simple Breit-Wigner (dashed); the dotted curve shows the cross section for $f_0(1300) \to 4\pi$; the dash-dotted curve shows the cross section for $f_0(1300) \to 4\pi$ with the phase space available in $\bar{p}p$ annihilation at rest.*

References

[1] P. Baillon *et al.* (CERN-College de France Collaboration), *Nuovo Cim.* **50A** (1967) 393.

[2] C. Edwards *et al.* (Crystal Ball Collaboration), *Phys. Rev. Lett.* **49** (1982) 259.

[3] C. Amsler *et al.* (Crystal Barrel Collaboration), *Phys. Lett.* **B358** (1995) 389.

[4] D. Urner, *PhD. Univ. Zürich.* (1995) unpublished.

[5] R. Bizzari *et al. Nucl. Phys.* **B14** (1969) 169.

[6] M. Foster *et al. Nucl. Phys.* **B8** (1968) 174.

[7] S. Spanier *CB-NOTE-310.*

[8] L. Montanet et al. *CB-Note-288*

[9] B.S. Zou and D.V. Bugg, Phys. Rev. D48 (1993) 3948.

[10] D.V. Bugg and B.S. Zou, Phys. Lett. B396 (1997) 295.

[11] Technical report on $\bar{p}p \to \eta\pi^0\pi^0\pi^0$, CB Note xxx.

[12] D.V. Bugg, V.V. Anisovich, A. Sarantsev and B.S. Zou, Phys. Rev. D50 (1994) 4412..

[13] C. Amsler et al., Phys. Lett. B358 (1995) 389.

[14] A. Bertin et al., Phys. Lett. B361 (1995) 187.

[15] Yu. D. Prokoshkin and S.A. Sadovsky, Nucl. Phys. B (Proc. Suppl.) 56A (1997) 222.

[16] A. Ostrovidov, E852 results, Hadron'97..

[17] A. Zaisev, VES results, Hadron'97.

[18] D.V. Bugg, A.V. Sarantsev and B.S. Zou, Nucl. Phys. B471 (1996) 59.

[19] A. Abele et al, Nucl. Phys. A609 (1996) 562.

[20] A. Abele et al., Phys. Lett. B380 (1996) 453.

[21] A. Abele et al., Phys. Lett. B385 (1996) 425.

[22] V.V. Anisovich et al., Phys. Lett. B355 (1995) 363.